Chem

Article

Bioluminescence-activated proximity labeling for spatial multi-omics

Graphical abstract

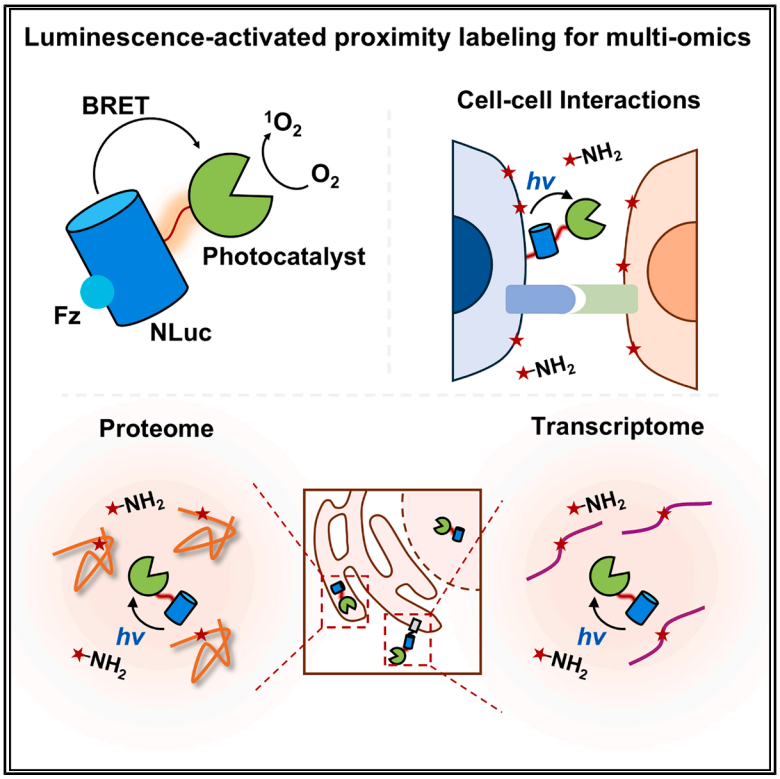

Highlights

- Biocompatible luminescence-activated proximity labeling for multi-omics
- High-specificity mapping of local proteomes *in vitro* and *in vivo*
- Selective capture of ligand-receptor-mediated cell-cell interactions
- High-coverage profiling of subcellular transcriptomes

Authors

Ruixiang Wang (王瑞祥), Yuxin Fang (方煜新), Youyue Hu (胡优粤), Yanjun Liu (刘衍军), Peng R. Chen (陈鹏), Peng Zou (邹鹏)

Correspondence

liuyanjun@mail.hzau.edu.cn (Y.L.), pengchen@pku.edu.cn (P.R.C.), zoupeng@pku.edu.cn (P.Z.)

In brief

Here, we introduce a biocompatible, BRET-activated proximity labeling platform that leverages luciferase-generated bioluminescence to drive photocatalytic tagging without external light, enabling high-resolution spatial proteome mapping, selective capture of ligand-receptor-mediated cell-cell interfaces, and precise subcellular transcriptome profiling in both *in vitro* and *in vivo* settings. By uniting the spatiotemporal control of photocatalysis with the physiological compatibility of luciferases, this strategy offers a versatile toolkit for interrogating complex biological processes with unrivaled spatial specificity.

Wang et al., 2025, Chem *11*, 102595
October 9, 2025
https://doi.org/10.1016/j.chempr.2025.102595

CellPress

Please cite this article in press as: Wang et al., Bioluminescence-activated proximity labeling for spatial multi-omics, Chem (2025), https://doi.org/10.1016/j.chempr.2025.102595

Chem

CellPress

Article

Bioluminescence-activated proximity labeling for spatial multi-omics

Ruixiang Wang (王瑞祥),[1,2,3,4,5,6,11] Yuxin Fang (方煜新),[1,2,3,4,5,6,11] Youyue Hu (胡优粤),[7] Yanjun Liu (刘衍军)[1,2,3,4,5,6,8,*] Peng R. Chen (陈鹏),[1,2,3,4,5,6,9,*] and Peng Zou (邹鹏)[1,2,3,4,5,6,9,10,12,*]

[1]College of Chemistry and Molecular Engineering, Peking University, Beijing 100871, China
[2]Synthetic and Functional Biomolecules Center, Peking University, Beijing 100871, China
[3]Beijing National Laboratory for Molecular Sciences, Peking University, Beijing 100871, China
[4]Key Laboratory of Bioorganic Chemistry and Molecular Engineering of Ministry of Education, Peking University, Beijing 100871, China
[5]PKU-IDG/McGovern Institute for Brain Research, Peking University, Beijing 100871, China
[6]Beijing Advanced Center of RNA Biology (BEACON), Peking University, Beijing, 100871, China
[7]Peking-Tsinghua-NIBS Joint Graduate Program, Peking University, Beijing 100871, China
[8]National Key Laboratory of Crop Genetic Improvement, Hubei Hongshan Laboratory, Huazhong Agricultural University, Wuhan 430070, China
[9]Academy for Advanced Interdisciplinary Studies, PKU-Tsinghua Center for Life Science, Peking University, Beijing 100871, China
[10]Chinese Institute for Brain Research (CIBR), Beijing 102206, China
[11]These authors contributed equally
[12]Lead contact
*Correspondence: liuyanjun@mail.hzau.edu.cn (Y.L.), pengchen@pku.edu.cn (P.R.C.), zoupeng@pku.edu.cn (P.Z.)
https://doi.org/10.1016/j.chempr.2025.102595

THE BIGGER PICTURE A detailed mechanistic picture of proteins, RNAs, and cells hinges on accurately mapping their spatial organization and interactions. Although photocatalytic proximity labeling (PL) offers spatiotemporally controlled tagging of biomolecules and cells, its reliance on external light limits deep-tissue applications in live animals. To address this, we harnessed luciferase-generated bioluminescence as an internal light source, obviating the need for external illumination.

We introduce a biocompatible, bioluminescence resonance energy transfer (BRET)-driven PL platform that enables spatially selective tagging at both the intracellular and intercellular levels *in vitro* and *in vivo*. By combining the high resolution of photocatalytic labeling with the physiological compatibility of luciferases, this toolkit paves the way for deep-tissue, high-resolution spatial omics in living systems.

SUMMARY

Mapping the spatial organization of proteins and cellular interactions is crucial for understanding their biological functions. Herein, we report a biocompatible, multi-functional luminescence-activated proximity labeling (LAP) strategy for profiling subcellular proteomes and cell-cell interactions in live cells and animals. Our method capitalizes on fusing the photocatalyst miniSOG to NanoLuc luciferase, whose bioluminescence activates miniSOG via a resonance energy transfer mechanism, generating reactive oxygen species *in situ* to mediate proximity labeling (PL). We demonstrated the high spatial specificity of LAP in a C57BL6/N mouse model transplanted with MC38 cells. Our data revealed tumor microenvironment-dependent remodeling of secretome. LAP was further applied to identify ligand-receptor-mediated cell-cell interactions both *in vitro* and *in vivo*. We also achieved local transcriptome profiling by combining LAP with next-generation sequencing. Overall, LAP was proved to be a versatile PL technique with strong biocompatibility for spatial multi-omic applications.

INTRODUCTION

The spatial organization of the intracellular proteome[1] (e.g., protein secretion,[2] assembly of membrane-less granules[3]) and intercellular interactions (e.g., T cell-dendritic cell interactions,[4] neuron-glial interactions[5]) are fundamental to virtually all life processes. Disruptions in protein localization or aberrant cellular interactions are closely linked to an array of human diseases, ranging from cancer[6,7] to neurodegeneration.[5,8] Therefore, a comprehensive understanding of the biological functions of

Please cite this article in press as: Wang et al., Bioluminescence-activated proximity labeling for spatial multi-omics, Chem (2025), https://doi.org/10.1016/j.chempr.2025.102595

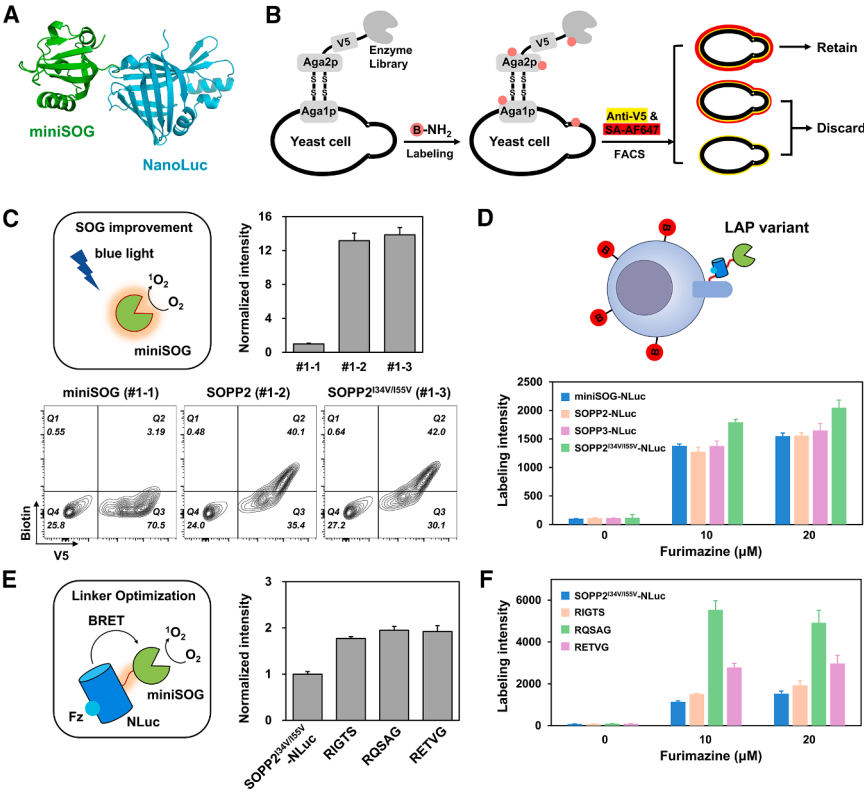

Figure 1. Development of LAP labeling method

(A) The structure of miniSOG-NanoLuc chimera.

(B) Schematic illustration of yeast display-directed evolution of LAP. Mutants are expressed on the yeast cell surface via fusion with the Aga2p protein. Following LAP labeling, cells with high levels of biotinylation are enriched with fluorescence-activated cell sorting (FACS).

(C and D) Flow cytometry analysis of LAP mutants on yeast cell surface (C) and HEK293T cell surface (D). Data are represented as mean ± SD (n = 3).

(E and F) Flow cytometry analysis of LAP linker variants on yeast cell surface (E) and HEK293T cell surface (F). Data are represented as mean ± SD (n = 3).

proteins and cells necessitates detailed knowledge of their spatial context.

To decipher spatial arrangements, various proximity labeling (PL) methods have been developed, which typically rely on an enzyme or photocatalyst to generate short-lived, highly reactive intermediates that label nearby biomolecules. While widely used, these methods still have limitations. For instance, APEX[9,10] labeling requires H_2O_2, which can be toxic to living cells and animals.[11] Biotin ligase-based methods (e.g., BioID[12] and TurboID[13]) offer better biocompatibility but suffer from uncontrolled labeling due to endogenous biotin[14,15] and perform poorly on the cell surface because of their ATP dependency.[16] Sortase-based PL methods (e.g., LIPSTIC[17,18] and EXCELL[17,18]) have significantly advanced *in vivo* studies of cell-cell interactions, but they are less effective for intracellular labeling. Recently, light-activated photocatalytic PL methods have been developed for both spatial proteomic and cellular interaction studies.[19] While light activation provides higher spatiotemporal resolution, the challenge of light penetration still limits their applications in living animals. These challenges motivated us to develop a biocompatible PL method for targeting both subcellular proteins and cell-cell interactions in living animals.

We envisioned that the light-activated photocatalytic PL methods could be expanded to address the challenge of delivering light into living animals. Given that the absorption spectrum of miniSOG[20] (λ_{max} = 448 nm) closely overlaps with the emission peak of NanoLuc (~460 nm), an ATP-independent luciferase derived from deep-sea shrimp *Oplophorus gracilirostris*,[21] we reasoned that fusing these two proteins may allow for miniSOG activation by NanoLuc through a bioluminescence resonance energy transfer (BRET) mechanism.[22] This would lead to the *in situ* generation of reactive oxygen species (ROS) that oxidize surrounding proteins, thereby triggering PL.[23–27] Although the NanoLuc-miniSOG complex has been used in photodynamic therapy for deep-seated tumors, it has not been applied for PL.[28] Similarly, while BRET has been used to activate LOV-Turbo to control TurboID activity, BRET-induced LOV-Turbo has not yet been employed for proteome mapping and is inactive in the secretory compartment of mammalian cells.[15]

Here, we report the engineering of the miniSOG-NanoLuc complex through directed evolution and its application in a luminescence-activated PL (LAP) strategy for profiling the intracellular proteome (LAP-MS). Spatial proteomic studies of the endoplasmic reticulum (ER) lumen and nucleus in human embryonic kidney 293T (HEK293T) cells demonstrated that LAP-MS can identify subcellular proteomes with high specificity and coverage. In a C57BL6/N mouse model implanted with MC38 cells expressing ER lumen-localized LAP, we confirmed the high efficiency of LAP-MS in capturing the tumor subcellular proteome *in vivo*. To further demonstrate its labeling capability on the cell surface, we developed the LAP-CELL method for identifying ligand-receptor-mediated cell-cell interactions both *in vitro* and *in vivo*. Finally, we combined LAP with next-generation sequencing to achieve local transcriptome profiling (LAP-seq). Collectively, our data establish LAP as a versatile, biocompatible PL technique for *in vivo* multi-omic studies.

RESULTS

Development of luminescence-activated PL method

To test the feasibility of BRET-assisted PL, we started with fusing NanoLuc directly to the C terminus of miniSOG (Figure 1A). The chimeric enzyme was genetically targeted to the mitochondrial

Please cite this article in press as: Wang et al., Bioluminescence-activated proximity labeling for spatial multi-omics, Chem (2025), https://doi.org/10.1016/j.chempr.2025.102595

matrix of HEK293T cells via fusion to the N-terminal localization sequence of human COX4 (Figure S1A). We treated the cells with 10 mM propargyl amine (PA) and 25 μM furimazine for 90 min, which yielded reliable labeling results, compared with negative controls that lacked either the PA probe or the furimazine substrate (Figure S1B). Adding flexible linkers between miniSOG and NanoLuc significantly reduced labeling efficiency, likely due to the increased distance between the donor and acceptor of the BRET pair. Additionally, fusing another NanoLuc to the N terminus of miniSOG did not further improve the labeling efficiency (Figures S1A and S1B).

Encouraged by our initial success, we aimed to improve the activity of the miniSOG-NanoLuc fusion through directed evolution. We chose yeast display as our platform since it has been effectively used to engineer PL enzymes, including APEX2[10] and TurboID,[13] often resulting in significantly enhanced activities (Figure 1B). In our initial rounds of selection, we ignored the NanoLuc part and focused solely on miniSOG variants with increased photocatalytic labeling efficiency under blue light irradiation (Figure 1C). To choose the starting point for directed evolution, we compared the activities of miniSOG and several previously reported mutants with higher singlet oxygen ($^1O_2$) quantum yields[29,30] (e.g., SOPP, SOPP2, and SOPP3). We found that SOPP2 exhibited the strongest labeling on the yeast surface (Figures S2A and S2B). Consequently, we generated a random mutagenesis library by error-prone PCR using SOPP2 as the template.

By fusing the SOPP2 mutant library to the Aga2p protein, we targeted the mutants to the surface of yeast cells. Upon the addition of a biotin-conjugated alkylamine probe (Btn-NH_2)[23] and irradiation with blue light at 15 mW/cm^2 for 5 s or 1 min, yeast cells expressing active mutants labeled themselves with biotin handles. We used fluorescence-activated cell sorting (FACS) to enrich cells with high levels of biotinylation (Figure 1B). After four rounds of selection, several mutants with enhanced labeling activities were identified by Sanger sequencing (Figures S3A and S3B). We manually combined mutations and expressed the resulting constructs in the HEK293T nucleus. Western blot analysis following labeling showed that the variant carrying the I34V/I55V double mutations exhibited the highest activity, outperforming miniSOG, SOPP2, and SOPP3 (Figure S3C). However, FACS analysis on the yeast surface indicated only a slight (1.1-fold) and statistically insignificant improvement of SOPP2$^{I34V/I55V}$ over SOPP2 (Figure 1C). Using the singlet oxygen sensor green (SOSG) probe, we measured the $^1O_2$ quantum yield of SOPP2$^{I34V/I55V}$ as 0.21, which is comparable to SOPP2 (0.21) but lower than SOPP3 (0.25) (Figure S3D). This suggests that factors beyond $^1O_2$ yield contribute to the overall labeling activity.

Next, we paired SOPP2$^{I34V/I55V}$ with NanoLuc. When targeted to the HEK293T cell surface by fusion with the membrane protein CD40L, the SOPP2$^{I34V/I55V}$-NanoLuc chimera exhibited 1.3- and 1.2-fold higher activity than SOPP2-NanoLuc ($p < 0.001$) and SOPP3-NanoLuc ($p < 0.01$), respectively, in the presence of 20 μM furimazine (Figure 1D). To further enhance BRET efficiency between SOPP2$^{I34V/I55V}$ and NanoLuc, we optimized the linker sequence. We generated a yeast expression library of fusion constructs with varying linker lengths by systematically truncating the termini of SOPP2$^{I34V/I55V}$ and NanoLuc (Figure S4A). The library explored two fusion strategies: (1) attaching NanoLuc to either the N or C terminus of SOPP2$^{I34V/I55V}$ and (2) incorporating a flexible Gly-Thr (GT) linker at the junction. Yeast cells expressing the mutant library were incubated with 10 μM furimazine and 50 μM Btn-NH_2 for 45 min and subsequently selected by FACS for high biotinylation efficiency (Figure S4B). Sequencing analysis identified the selected mutant as NanoLuc-GT-SOPP2$^{I34V/I55V}$ fusion with two amino acids truncated from both the C terminus of NanoLuc and the N terminus of SOPP2$^{I34V/I55V}$ (Figure S4C). This construct exhibited 1.77-fold higher labeling efficiency than SOPP2$^{I34V/I55V}$-NanoLuc (Figure 1E).

To further optimize the relative orientation of the BRET pairs, we randomized the linker sequence by performing saturation mutagenesis on five amino acid residues at the junction, including: the GT linker, two residues on its N-terminal side, and one on its C-terminal side (Figure S5A). These sites, located in loop regions, preserved the structural integrity of the proteins. Following a similar yeast display selection workflow, we identified two linker sequences, RQSAG and RETVG (Figure S5B and S5C), with 1.10- and 1.08-fold improvement, respectively, compared with the initial template (RIGTS) (Figure 1E). When expressed on the HEK293T cell surface, the mutant with the RQSAG linker showed the highest activity, achieving 4.8-fold stronger labeling than SOPP2$^{I34V/I55V}$-NanoLuc with 10 μM furimazine (Figure 1F). We designated this optimized construct, which incorporates the RQSAG linker, as LAP and used it for subsequent experiments. Targeting key mutants to the HEK293T cytosol confirmed that LAP performs significantly better than the initial miniSOG-NanoLuc construct (Figure S6A).

Using AlphaFold3,[31] we predicted the structure of LAP and measured the donor-acceptor distance as 3.16 nm, which was appropriate for the BRET process[22] (Figure S6B). We then recorded the emission spectra of purified NanoLuc and LAP proteins in the presence of furimazine. LAP's emission peak was red-shifted by approximately 20 nm relative to NanoLuc (Figure S6C), with LAP peaking at 475 nm, which is consistent with the emission profile of SOPP2$^{I34V/I55V}$ (Figure S6D). We calculated a BRET ratio of 0.357 ± 0.012, confirming the LAP mechanism. The production of $^1O_2$ was monitored using the SOSG probe. Following the addition of furimazine in the presence of LAP, we observed an increase in fluorescence emission, indicating the successful generation of $^1O_2$. Interestingly, NanoLuc was also able to produce $^1O_2$ independently, albeit with a lower yield (Figure S6E). To further validate the labeling mechanism, we treated HEK293T cells expressing LAP or NanoLuc localized in the ER lumen with a 3-ethynylaniline (3-EA) probe[26] and 50 μM furimazine for 2 h, followed by western blot analysis. Cells expressing LAP displayed significant protein labeling, in contrast to the weaker signal from cells expressing NanoLuc alone (Figure S6F). These results underscore the critical role of the BRET mechanism in activating photocatalysts for PL, while the modest labeling observed with NanoLuc alone suggests potential for further optimization.

Please cite this article in press as: Wang et al., Bioluminescence-activated proximity labeling for spatial multi-omics, Chem (2025), https://doi.org/10.1016/j.chempr.2025.102595

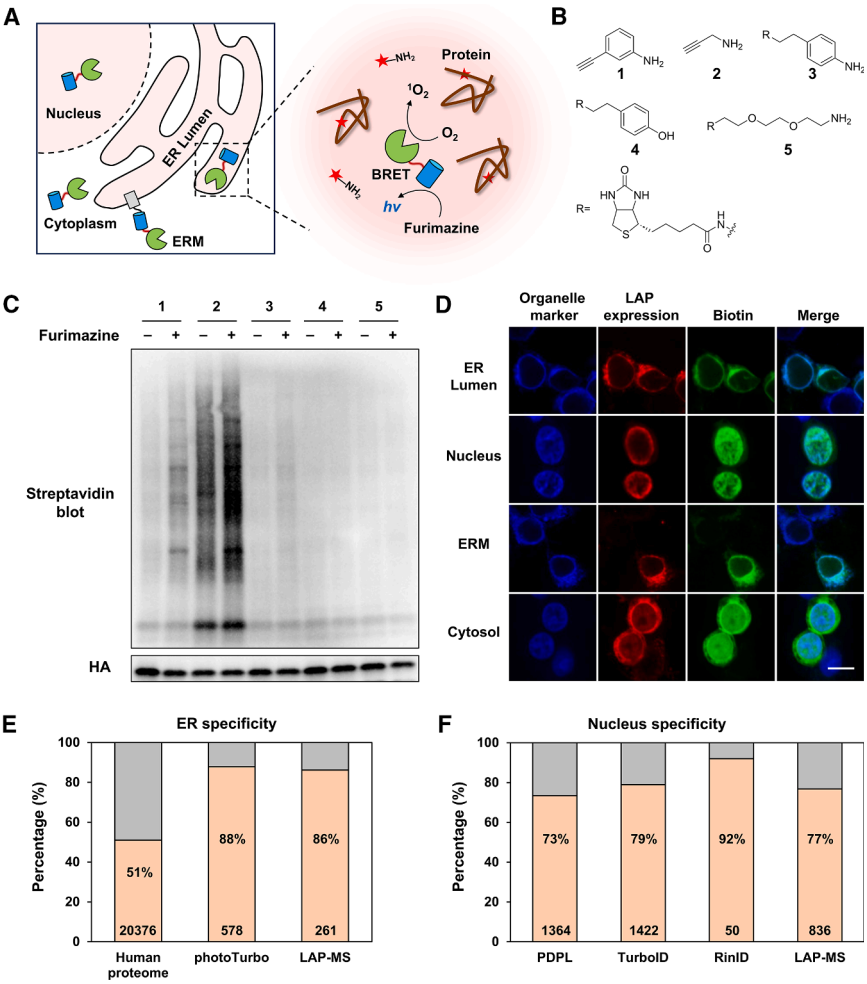

Figure 2. Mapping subcellular proteome with LAP-MS in living cells

(A) Targeting of LAP at ER lumen, nucleus, ER membrane (ERM), and cytoplasm for subcellular proteome labeling.

(B) Chemical structures of probes used for protein labeling.

(C) Western blot analysis comparing protein labeling activity of different probes (LAP was fused with HA tag).

(D) Confocal fluorescence images of HEK293T cells labeled with LAP in ER lumen, nucleus, ERM, and cytoplasm. Scale bar: 10 μm.

(E and F) Comparisons of secretory pathway specificity (E) and nucleus specificity (F) of LAP-MS with various proximity labeling methods.

Mapping subcellular proteome with LAP-MS in cultured cells

We aimed to achieve LAP-mediated subcellular protein labeling in live cells. To this end, we generated HEK293T cell lines expressing LAP targeted to various subcellular compartments, including the cytoplasm, ER lumen, ER membrane, and nucleus (Figure 2A). In parallel, we prepared several amine probes to evaluate labeling efficiency: 3-EA (**1**), PA (**2**), biotin-aniline (BA, **3**), biotin-phenol (BP, **4**), and Btn-NH_2 (**5**) (Figure 2B). HEK293T cells expressing ER lumen-targeted LAP were incubated with each probe along with 50 μM furimazine for 2 h, followed by protein extraction and western blot analysis. Although PA (probe **2**) yielded the highest labeling intensity, it also produced high background in the absence of furimazine. Therefore, we selected 3-EA (probe **1**) for its optimized balance between labeling efficiency and background (Figure 2C).

To evaluate the spatial specificity of LAP-mediated protein labeling, we performed immunofluorescence imaging of cell samples labeled with 3-EA. After initiating the reaction with 50 μM furimazine for 2 h, cells were fixed and permeabilized with cold methanol. The biotinylation signal was then detected by staining cells with streptavidin-conjugated fluorophores, while the localizations of LAP and organelles were visualized via antibody staining (or DAPI staining for the nucleus). Confocal fluorescence microscopy revealed good co-localization between the biotinylation signal and organelle markers, demonstrating the high spatial specificity of LAP-mediated protein labeling (Figure 2D). Notably, the intrinsic green fluorescence of LAP was also detectable at the anticipated locations, although at low intensity (Figure S7A). Western blot analysis confirmed successful labeling across multiple subcellular compartments, including the cytoplasm, ER lumen, nucleus, ER membrane, and cell membrane (Figure S7B).

We next characterized the temporal resolution of LAP-mediated protein labeling. HEK293T cells expressing ER lumen-targeted LAP were incubated with 1 mM 3-EA probe and 50 μM furimazine for varying durations. Immunoblotting revealed that labeling was detectable after just 15 min, with a stronger labeling observed after 2 h (Figure S7C). Moreover, by adding or removing furimazine, we could effectively switch the labeling on and off, demonstrating the temporal control of the LAP approach (Figure S7D). In a comparison of labeling methods, LAP-expressing cells treated with 1 mM 3-EA and 50 μM furimazine for 2 h exhibited significantly lower BRET-mediated labeling efficiency than cells irradiated with blue light at 15 mW/cm^2 for comparable durations (Figure S7E), suggesting that bioluminescence generation and energy transfer constrain BRET activation. To assess cytotoxicity, we performed a cell proliferation assay. After 2 h of labeling with 1 mM 3-EA and 50 μM furimazine, LAP-expressing cells showed only slight, statistically insignificant cytotoxic effect (Figure S7F).

Having fully characterized LAP-mediated protein labeling, we applied LAP to map the local proteome using quantitative MS-based proteomic profiling (LAP-MS). HEK293T cells expressing LAP targeted to either the ER lumen or the nucleus-localized LAP were labeled with 1 mM 3-EA probe and 50 μM furimazine for 2 h, followed by cell lysis and protein extraction. The labeled proteins were reacted with biotin-conjugated azide via a click reaction

Please cite this article in press as: Wang et al., Bioluminescence-activated proximity labeling for spatial multi-omics, Chem (2025), https://doi.org/10.1016/j.chempr.2025.102595

and captured using streptavidin-coated agarose beads. Successful protein enrichments were confirmed by SDS-PAGE for both the ER lumen and nucleus (Figure S7G). After liquid chromatography-tandem mass spectrometry (LC-MS/MS) analysis, we identified and quantified the ER lumen proteome in replicates for "+/− furimazine," revealing 261 proteins, of which 225 were secretory pathway proteins according to RinID[25] work (Figure S8A). The secretory pathway specificity of our ER lumen dataset (86%) is comparable to photoTurbo[14] (88%) (Figure 2E; Data S1), while we identified a greater number of ER resident proteins (Figure S8B). Similarly, the nuclear proteome was identified and quantified in replicates for +/− furimazine, revealing 836 proteins, with 644 classified as nuclear proteins according to RinID[25] work (Figure S8C; Data S2). The nucleus specificity of our dataset (77%) is comparable to PDPL[26] and TurboID,[13] although RinID[25] showed higher specificity (92%) but with relatively low coverage (Figure 2F). Taken together, these LC-MS/MS data demonstrate that LAP-MS can identify subcellular proteomes with high specificity and good coverage.

Mapping subcellular proteome with LAP-MS in live animals

The success of applying LAP-MS to label subcellular proteome in cultured cells encouraged us to extend this approach to identify subcellular proteome in living animals. We focused on the cancer immunoediting process, which describes the dynamic interplay between cancer cells and the immune systems during tumor progression. To evade immune invasion, cancer cells remodel their surface proteins and secreted proteins, prompting us to capture and identify the tumor secretary pathway proteome within tumor microenvironment.[7] MC38 is a widely used immunoresponsive murine colon adenocarcinoma model,[32,33] making it suitable for *in vivo* secretome studies.

To obtain tumor-bearing mice for *in vivo* secretome labeling, we constructed an MC38 cell line stably expressing LAP targeted to the ER lumen. Immunofluorescence imaging (Figure S9A) confirmed the labeling specificity in the MC38 cell line labeled with the 3-EA probe. The secretome of cultured MC38 cells was enriched and identified using quantitative MS-based proteomic profiling. Proteins were ranked by their +/− furimazine ratios in each replicate, with cutoff ratios determined using receiver operating characteristic (ROC) analysis (Figure S9B). The "true-positive" and "false positive" murine secretome lists were created based on methods from previous TurboID[13] studies, resulting in 87 annotated secretory pathway proteins and 7,296 non-secretory pathway proteins. The cutoff ratios were set at 2.96, 3.10, and 2.80, yielding 174, 181, and 214 enriched proteins for the three +/− furimazine datasets, respectively. Venn diagram analysis revealed that 177 proteins were identified in at least 2 replicates, including 158 secretory pathway proteins (89%) (Figure S9C; Data S3). The LC-MS/MS data demonstrated the LAP-MS method's capability to identify subcellular proteomes in MC38 cells, laying a solid foundation for *in vivo* secretome labeling in mouse tumors.

The MC38 cells expressing ER lumen-targeted LAP were subcutaneously implanted into mice to generate solid tumors. Secretome labeling was initiated *in situ* by intratumoral injection of the 10 mM 3-EA probe and 4 mM furimazine (Figure 3A). After a 2-h reaction, tumor tissues were isolated and lysed using RIPA buffer. The labeled proteins were then reacted with biotin-conjugated azide via click reaction and characterized by SDS-PAGE. Western blot analysis revealed successful *in vivo* protein labeling in a furimazine-dependent manner (Figure 3B). The tumor secretome was enriched and identified with quantitative MS-based proteomic profiling. Following a similar data analysis workflow of ROC analysis (Figure S9D), a total of 136 proteins were identified in at least 2 replicates, including 107 secretory pathway proteins (79%) (Figure 3C; Data S4).

Comparison of secretary pathway proteins identified in cultured cells and murine tumors revealed that the tumor-specific dataset contained fewer ER resident proteins and a higher proportion of extracellular proteins and membrane proteins. These proteins likely contribute to tissue formation and cell-cell communications within the tumor microenvironment (Figure 3D). Taken together, our results demonstrate the high efficiency of LAP-MS for profiling the tumor subcellular proteome *in vivo* and provide new insights into secretome remodeling driven by the tumor microenvironment.

Detecting cell-cell interactions via LAP-CELL

We expanded the application of LAP-mediated protein labeling to map cell-cell interactions, a method we refer to as LAP-CELL. First, two biotin-conjugated amine probes (BA and Btn-NH_2) were evaluated on HEK293T cell surfaces. FACS analysis revealed that the BA probe exhibited stronger self-labeling activity (Figure S10A), and it was therefore selected for LAP-CELL. Cell proliferation assay further confirmed that labeling with 100 μM BA probe and 20 μM furimazine did not induce significant cytotoxicity (Figure S10B).

Next, we employed the CD40/CD40L interaction as a model.[34] HEK293T cells were transfected separately with CD40L-LAP (bait), CD40 (prey), or EGFP (negative control). Cells expressing CD40L-LAP were mixed with either CD40 cells or EGFP cells, incubated with 100 μM BA probe and 20 μM furimazine substrate for 45 min, stained with streptavidin-conjugated fluorophore, and then analyzed by flow cytometry (Figure 4A). Substantial amount of *cis*-labeling of CD40L-LAP cells were observed, regardless of whether they were mixed with CD40 cells or EGFP cells (Figure S10C). For *trans*-labeling, CD40 cells showed high levels of biotin signal, whereas EGFP cells had much lower labeling under identical conditions (Figure 4B). These results confirmed that LAP-CELL can label interaction-dependent cellular interactions with high specificity.

Recently, chimeric antigen receptor T (CAR-T) therapy has shown remarkable efficacy in treating hematologic malignancies.[35,36] We wondered whether LAP-CELL could capture CAR-interacting cells. Anti-CD19 CARs, which are commonly used for treating B cell lymphomas,[37] were utilized in our study. We established a cell line stably expressing both anti-CD19 CAR and cell membrane-localized LAP to capture CD19-positive cells, such as Raji cells (Figure 4C).

To assess LAP-CELL's sensitivity in labeling CAR-interacting cells, we mixed CD19-negative K562 cells with CD19-positive Raji cells at different ratios (1:1, 10:1, and 100:1). The mixed cells were then incubated with an equal number of bait cells in the

Please cite this article in press as: Wang et al., Bioluminescence-activated proximity labeling for spatial multi-omics, Chem (2025), https://doi.org/10.1016/j.chempr.2025.102595

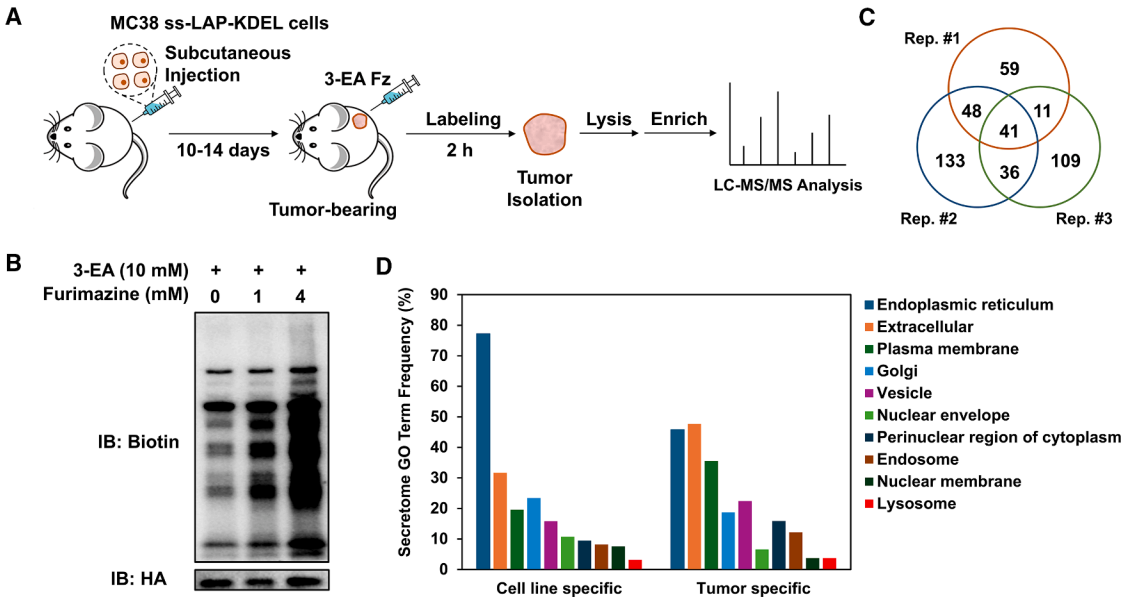

Figure 3. Mapping ER lumen proteome with LAP-MS in living mice

(A) Schematic illustration of *in vivo* mapping of ER lumen proteome in tumors with LAP-MS. The MC38 cells expressing ER lumen-targeted LAP were subcutaneously implanted into mice to generate solid tumors, followed by intratumoral injection of 3-EA probe and furimazine (Fz) to trigger proximity labeling. Subsequently, tumor cells were excised and lysed before being subject to LC-MS/MS analysis.

(B) Western blot analysis of LAP-mediated ER lumen proteome labeling in murine tumor (LAP was fused with HA tag).

(C) Tumor ER lumen proteome identification with LAP-MS in 3 replicates for +/− furimazine; a total of 136 proteins were detected from three independent LAP-MS experiments.

(D) Gene Ontology analysis of secretary pathway proteins identified in cultured cells and murine tumors.

presence of 100 μM BA probe and 20 μM furimazine for 45 min (Figure 4C). Flow cytometry analysis revealed robust *trans*-biotinylation on Raji cells, with minimal background labeling on K562 cells (Figure 4D). Notably, even when Raji cells were present at low abundance, their labeling efficiency remained high, underscoring LAP-CELL's capability to capture rare interacting cells.

To assess the *in vivo* compatibility of LAP-CELL for capturing cell-cell interactions, we mixed two populations of HEK293T cells expressing either CD40L-LAP or CD40 and intraperitoneally injected them into mice. After 15 min, we administered 500 μL of PBS solution containing 300 μM furimazine and 1 mM BA probe to the mice to trigger cellular labeling for 45 min, followed by cell isolation and flow cytometry analysis (Figure 4E). CD40L-LAP cells were also co-cultured with EGFP-expressing cells as a negative control. Flow cytometry showed specific *trans*-biotinylation on CD40-positive cells, with negligible labeling background on EGFP control cells (Figure 4F). This experiment demonstrated that LAP-CELL can capture cellular interactions *in vivo* with high specificity. In summary, we have demonstrated the capacity of LAP-CELL to detect ligand-receptor-directed cell-cell interactions (e.g., CD40-CD40L and CD19-Anti-CD19 CAR) both *in vitro* and *in vivo*.

Transcriptomic profiling with LAP-seq in the secretory pathway

In addition to labeling subcellular proteins, both intracellular and on the cell surface, we further developed LAP-mediated RNA labeling for profiling subcellular transcriptomes (LAP-seq). We focused on the ER membrane (ERM) location, where secretory pathway proteins are initially synthesized,[2] expecting to enrich mRNAs encoding the secretome at ERM. Unlike the ER lumen or nucleus, the ERM is a relatively "open" space, thus representing a more rigorous test for the spatial specificity of LAP labeling techniques.

To characterize LAP-seq's ability to identify the ERM-proximal transcriptome, we created a HEK293T cell line stably expressing LAP targeted to the ERM by fusing it to the N terminus of the ER translocon subunit Sec61β. Immunofluorescence imaging confirmed the spatial specificity of LAP-mediated protein labeling with the 3-EA probe in ERM-LAP cells (Figure 2D). For RNA labeling, we selected the PA probe based on chromophore-assisted proximity labeling and sequencing (CAP-seq)[23] protocols. ERM-LAP cells were incubated with 10 mM PA probe and 50 μM furimazine for 15–60 min, followed by cell lysis and RNA extraction. The labeled RNAs were then reacted with biotin-conjugated azide via click reaction, captured using streptavidin-coated magnetic beads, and characterized with dot blot (Figure S11A) and RT-qPCR analysis (Figure 5A). As expected, RNA recovery increased with longer reaction times. At 30 and 60 min, RNAs from secretary pathway genes (e.g., *SSR2* and *TMX1*) were enriched 47- to 112-fold, compared with controls lacking furimazine, whereas mitochondrial (*MTCO2*, 8- to 13-fold) and cytosolic (*FAU*, 24- to 26-fold) RNA markers showed only modest enrichment. Additionally, cell proliferation assay indicated minimal cytotoxicity in ERM-LAP cells following 60 min of labeling (Figure S11B).

Please cite this article in press as: Wang et al., Bioluminescence-activated proximity labeling for spatial multi-omics, Chem (2025), https://doi.org/10.1016/j.chempr.2025.102595

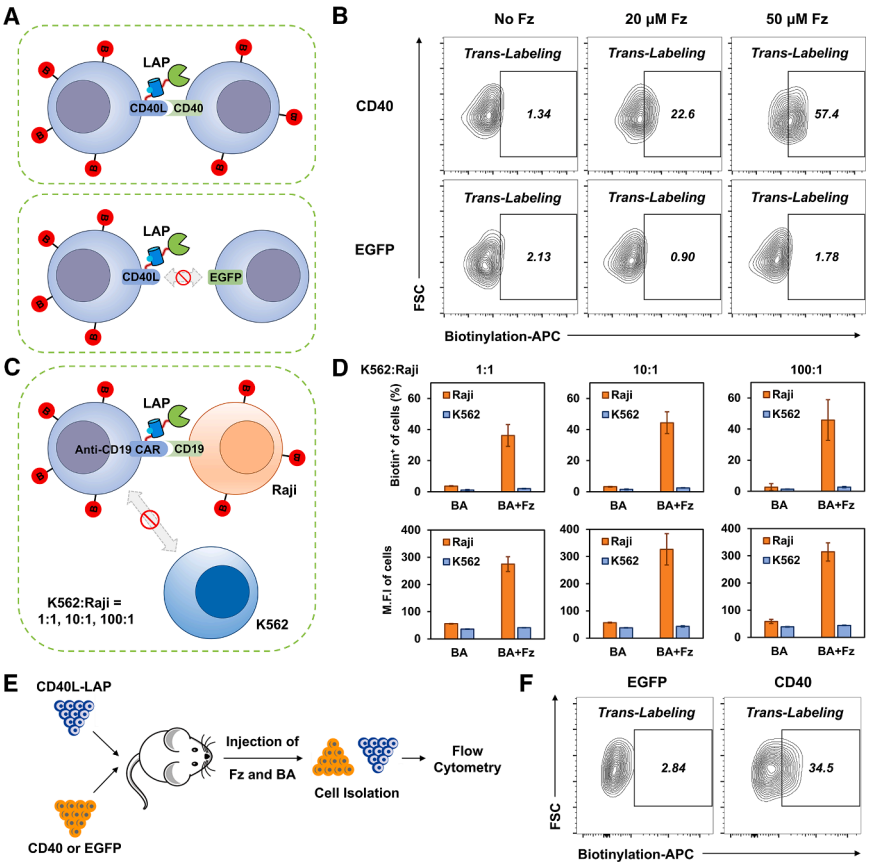

Figure 4. Detection of cell-cell interactions via LAP-CELL

(A) Experimental setup to identify CD40-CD40L-mediated cell-cell interactions via LAP-CELL. HEK293T cells expressing CD40L-LAP were mixed with either CD40 cells or EGFP cells, followed by addition of biotin-aniline (BA) probe and furimazine to trigger intercellular labeling.

(B) Flow cytometry analysis of *trans*-labeling efficiency of CD40 cells and EGFP cells.

(C) Experimental setup to capture anti-CD19 CAR-interacting cells via LAP-CELL. CD19-positive Raji cells and CD19-negative K562 cells were mixed at different ratios, followed by incubation with HEK293T cells expressing both anti-CD19 CAR and cell membrane-localized LAP.

(D) Flow cytometry analysis of LAP-CELL labeling efficiency. Mean fluorescence intensities are shown with error bars representing the biotin signal on cell surface. Data are represented as mean ± SD (n = 3).

(E) Workflow of labeling of CD40-CD40L-mediated cell-cell interactions *in vivo*. Two populations of HEK293T cells expressing either CD40L-LAP or CD40 were mixed and intraperitoneally injected into mice, followed by injection of BA probe and furimazine (Fz) to trigger *in vivo* labeling.

(F) Flow cytometry analysis of cells labeled in (E), where EGFP cells were set as control.

We further evaluated the spatial specificity and sensitivity of LAP-seq at the transcriptome level. In three independently replicated experiments, enriched RNAs were analyzed with next-generation sequencing. We applied DESeq2[38] analysis to compare the transcript abundance between labeled samples and control samples that omitted the furimazine substrate (Figure 5B). By applying a cutoff of $\log_2$ fold change ($\log_2$FC) > 1 and adjusted p (p_{adj}) < 0.05, the analysis yielded a list of 839 RNAs, including 831 mRNAs (99%), 6 pseudogenes, 1 antisense RNA, and 1 long noncoding RNA (Data S5). Notably, as a demonstration of LAP's high spatial specificity, 97.1% of enriched mRNAs (807 out of 831) encode for secretome proteins, which is expected from the model of localized protein translation on the ERM.[23] This level of specificity is comparable to CAP-seq[23] (96%), proximity ribosome profiling[39] (97%), and APEX-RNA immunoprecipitation (APEX-RIP)[40] (94%) (Figure 5C). Furthermore, 28%, 54%, and 98% of the transcripts identified by ERM LAP-seq (228, 437, and 793 out of 807, respectively) overlapped with datasets from CAP-seq,[23] proximity ribosome profiling,[39] and APEX-RIP[40] experiments, respectively (Figure 5D). Similar RNA labeling at the ERM was also verified in a MC38 cell line (Figures S11C–S11F; Data S6).

To explore the *in vivo* compatibility of LAP-seq, MC38 ERM-LAP cells were subcutaneously implanted into mice to form solid tumors. Labeling reaction was initiated by intratumoral injection of the PA probe and furimazine. After 1 h, RNA was extracted from the tumors and enriched. RT-qPCR analysis revealed significant enrichment of the secretary pathway RNA marker calnexin (*CANX*), while the cytosolic marker *FAU* showed no obvious enrichment (Figure S11G). Notably, this *in vivo* RNA labeling capability could not be readily achieved by current RNA labeling methods (CAP-seq,[23] proximity ribosome profiling,[39] and APEX-RIP[40]), which are limited by requirements for blue light, biotin starvation, or H_2O_2, respectively. Moreover, although TurboID has broad utility in *in vivo* protein labeling, it exhibits limited RNA labeling efficiency (Figure S12). In summary, our results demonstrate that LAP-seq robustly identify subcellular transcriptomes with high specificity and coverage, thereby complementing LAP-mediated protein labeling techniques.

DISCUSSION

Recent advances in photocatalytic PL have harnessed light activation to eliminate toxic reagents (e.g., H_2O_2) and enable precise temporal control of the reaction.[19] Although these methods have been successfully applied to both intracellular[23–27,41–47] and intercellular[48–50] spatial omics, their *in vivo* use is limited by the poor tissue penetration of light. In this study, we developed a LAP strategy that maps the spatial distribution of proteins and cell-cell interactions in living organisms. By integrating rational design with yeast display-directed evolution, we optimized LAP for enhanced labeling activity. Our

Please cite this article in press as: Wang et al., Bioluminescence-activated proximity labeling for spatial multi-omics, Chem (2025), https://doi.org/10.1016/j.chempr.2025.102595

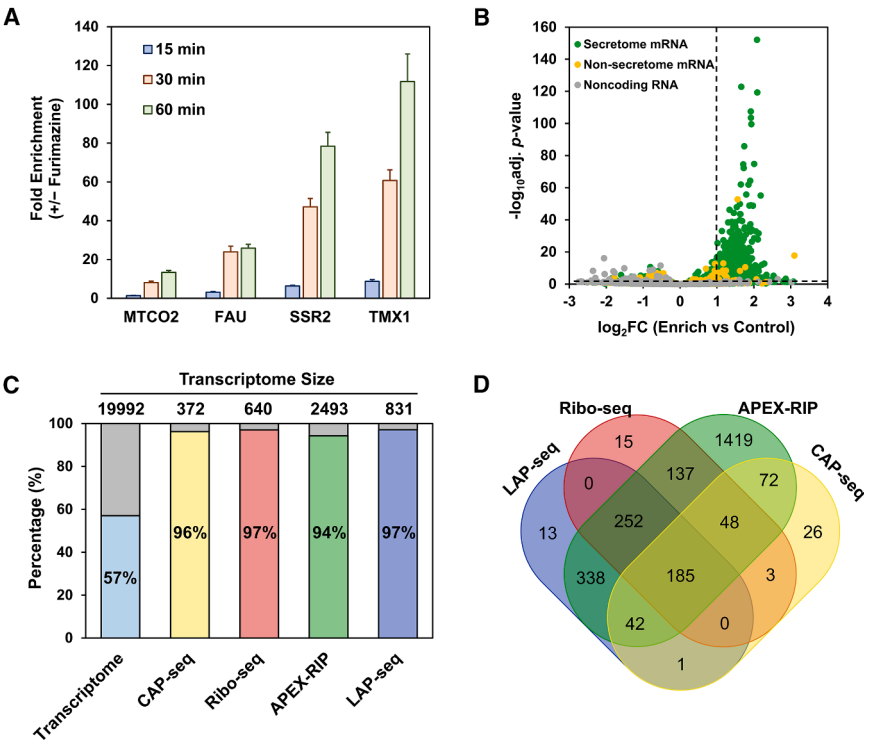

Figure 5. Transcriptomic profiling with LAP-seq in the secretory pathway

(A) RT-qPCR analysis of RNA labeling efficiency and specificity via LAP-seq. Data are represented as mean ± SD (n = 4).

(B) Volcano plot of the ERM LAP-seq dataset. Green, red, and black dots represent secretome mRNAs, non-secretome mRNAs, and noncoding RNAs, respectively. Horizontal dashed line indicates p_{adj} = 0.05. Vertical dashed line indicates the cutoff of $\log_2$(label vs. control) = 1.

(C) Comparisons of secretary pathway specificity of LAP-seq transcriptomic data with three other proximity labeling methods (proximity ribosome profiling [Ribo-seq], APEX-RIP, and CAP-seq).

(D) Venn diagram comparing the datasets of ERM LAP-seq, Ribo-seq, APEX-RIP, and CAP-seq.

results demonstrate that LAP can identify local proteomes with exceptional specificity and coverage across diverse cell types and subcellular compartments. In an MC38 tumor mouse model, LAP not only efficiently mapped the tumor subcellular proteome *in vivo*, but it also accurately labeled cell-cell interactions both *in vitro* and in living animals. Moreover, combining LAP with next-generation sequencing enabled local transcriptome profiling.

Conventional optogenetic approaches generally require invasive light-delivery methods, such as surgically implanted light-emitting devices, to overcome tissue penetration challenges.[15,51] In contrast, BRET-based optogenetic systems, such as the LuminON technique that fuses NanoLuc with LOV2 to control gene expression in living mice,[52] offer a less invasive alternative. Instead of relying on the conformational changes induced by BRET-activated LOV domains, as seen in LuminON and LOV-Turbo,[15] our LAP approach leverages bioluminescence to directly activate $^1O_2$ generators (e.g., miniSOG). Although BRET-activated ROS generation has been applied in photodynamic therapy for deep-seated tumors,[28] those methods previously required exogenous riboflavin mononucleotide as an flavin mononucleotide (FMN) source. In our LAP system, endogenous FMN levels are sufficient, thereby reducing off-target labeling and cellular toxicity.

Although miniSOG was originally designed as a $^1O_2$ generator, its $^1O_2$ quantum yield was later reported to be as low as 0.03.[29] Its photocatalytic efficiency could potentially be enhanced by introducing mutations at sites near the flavin mononucleotide chromophore.[29,30] Additionally, random mutagenesis of the miniSOG backbone can help identify critical sites that are challenging to predict through rational design. In our study, fusing NanoLuc with the SOPP2$^{I34V/I55V}$ mutant yielded higher activity than miniSOG and SOPP2. Moreover, optimizing the linker length and composition between NanoLuc and SOPP2$^{I34V/I55V}$ through saturation mutagenesis significantly boosted labeling efficiency.

We envision that LAP-MS, LAP-seq, and LAP-CELL techniques will have broad applications in studying protein secretion, organ-specific subcellular proteomes/transcriptomes, and *in situ* cell-cell interactions (e.g., tumor-immune or neuron-glial interactions). A current limitation of the LAP method is that its labeling efficiency is lower than that of light-triggered reactions, potentially affecting data reliability. Future improvements may include evolving NanoLuc for increased brightness, optimizing its substrates for better solubility and bioavailability, and designing more active labeling probes tailored to specific applications.

METHODS

Reagents

All the information about the reagents, antibodies, plasmids, and primers used in this work can be found in Tables S1–S4, separately.

Yeast cell culture

The *S. cerevisiae* strain EBY100 was a kind gift from Tao Liu's group, Peking University. Yeast cells were transformed with the yeast-display plasmid pCTCON2 using the Frozen E-Z Yeast Transformation II kit (Zymoprep) according to manufacturer protocols. Transformed cells containing the TRP1 gene were selected on synthetic dropout without uracil and tryptophan (SD-Ura-Trp) plates and propagated in SD-Ura-Trp medium at 30°C. The SD-Ura-Trp medium was composed of 20 g/L glucose, 6.7 g/L yeast nitrogen base without amino acids (BD Difco), and 1.46 g/L synthetic yeast dropout mix (Sigma-Aldrich, Y1771) supplemented with 0.38 g/L leucine. Protein expression was induced by inoculating saturated yeast culture into yeast extract peptone galactose (YPG) medium (20 g/L

Please cite this article in press as: Wang et al., Bioluminescence-activated proximity labeling for spatial multi-omics, Chem (2025), https://doi.org/10.1016/j.chempr.2025.102595

galactose, 20 g/L peptone, and 10 g/L yeast extract) at a 1:50 dilution and incubating at 30°C for 20 h.

Generation of mutant libraries for yeast display

The random mutation library starting from SOPP2 was generated by error-prone PCR. In a 100 μL reaction system, 20 ng of template DNA (containing the SOPP2 sequence only) was amplified for 20 cycles, with 0.4 μM forward (Err1_F) and reverse primers (Err1_R), 0.2 mM dNTPs, 2 mM $MgCl_2$, 2 μM 8-oxo-dGTP, 2 μM dPTP, and 0.1 U/μL Taq DNA polymerase. The PCR products were purified with the Zymo DNA Clean & Concentrator-5 kit. 1 μL of the first round PCR product was used as the template and was amplified for another 20 cycles, with 0.4 μM forward (Err2_F) and reverse primers (Err2_R) and with the 8-oxo-dGTP and dPTP removed from the reaction system. The PCR products were purified with the Zymo DNA Clean & Concentrator-5 kit and amplified for another 35 cycles under regular PCR conditions for the attachment of homologous arms. The 3rd PCR used the Pfu DNA polymerase, 0.4 μM forward (Homo_F), and reverse primers (Homo_R).

Before yeast electroporation, the inserts were ligated with the BamHI-NheI linearized pCTCON2 vector with the Lightning DNA assembly mix (Biodragon) and transformed into the *E. coli* strain DH5α for a small-scale sequencing validation. Next, 5 μg inserts was mixed with 1 μg vectors and further purified by ethanol precipitation. The DNA pellet was re-dissolved with 10 μL double-distilled H_2O (ddH_2O) and electroporated into electrocompetent EBY100 cells (one pulse with the BioRad MicroPulser electroporator in the fungi-sc2 mode, 1.5 kV initial voltage, and 5 ms time constant). The electrocompetent yeast cells were prepared by a typical LiAc/sorbitol protocol, in which 25 mL yeasts (OD_{600} = 2.5–3.0) was incubated with 12.5 mL 100 mM LiAc and 10 mM DTT at 30°C for 12 min, washed once with 12.5 mL 1 M ice-cold sorbitol, and then resuspended in 250 μL 1 M ice-cold sorbitol. The electroporated cultures were rescued in 2 mL yeast extract peptone dextrose (YPD) complete medium (20 g/L glucose, 20 g/L peptone, and 10 g/L yeast extract) for 1 h at 30°C with no shaking. The rescued cell suspension was transferred to 100 mL of SD-Ura-Trp medium and grown for 24–36 h at 30°C. 10 μL of the rescued cell suspension was diluted 100×, 1,000×, 10,000×, and 100,000×. 20 μL diluted cell suspension was plated on SD-Ura-Trp plates and incubated at 30°C for 3 days. After 3 days, each colony observed in the 100×, 1,000×, 10,000×, or 100,000× segments of plates will correspond to 10^4, 10^5, 10^6, or 10^7 transformants in the library, respectively.

The linker truncation library was generated by T4 ligation. The $SOPP2^{I34V/I55V}$ fragments and NanoLuc fragments with truncations at the N or C terminus were prepared individually by PCR amplification using the corresponding primers. For each construct, a short flexible linker Gly-Thr (containing the restriction endonuclease KpnI recognition site GGTACC) was added to the junction of $SOPP2^{I34V/I55V}$ and NanoLuc. A BamHI recognition sequence was added to the N terminus of the N-terminal inserts, and an NheI recognition sequence was added to the C terminus of the C-terminal inserts. The linearized pCTCON2 vectors were then ligated either with the N-terminal $SOPP2^{I34V/I55V}$ and C-terminal NanoLuc or with the N-terminal NanoLuc and C-terminal $SOPP2^{I34V/I55V}$ using a T4 ligase. The ligation mix was transformed into the *E. coli* strain DH5α and plated on Luria broth (LB) plates supplemented with 70 mg/L ampicillin. After 16 h of incubation at 37°C, colonies were collected and lysed for plasmid extraction. 0.6 μg plasmids expressing NanoLuc-linker library-$SOPP2^{I34V/I55V}$ and 0.6 μg plasmids expressing $SOPP2^{I34V/I55V}$-linker library-NanoLuc were concentrated by ethanol precipitation and electroporated into electrocompetent EBY100 cells, following the same protocol described above.

The linker sequence randomization library was generated by site-saturated mutagenesis. Five amino acid residues around the Gly-Thr junction, including two sites to its N terminus and one site to its C terminus, were simultaneously mutated via PCR with a forward primer containing five NNK degenerate codons and a reverse primer designed to base pair with the 3′ terminus of $SOPP2^{I34V/I55V}$ sequence. The $SOPP2^{I34V/I55V}$ fragment containing five randomized sites at the 5′ terminus was ligated to its N terminus with the NanoLuc fragment via an overlap PCR. The PCR products were purified with the Zymo DNA Clean & Concentrator-5 kit. 5 μg inserts was mixed with 1 μg BamHI-NheI linearized pCTCON2 vectors and further purified by ethanol precipitation. The DNA pellet was re-dissolved dissolved in 10 μL ddH_2O and electroporated into electrocompetent EBY100 cells, following the same protocol described above.

Please refer to Table S4 for a list of primers used for mutant library construction in this study.

Yeast display-based directed evolution

For each round of selection, 10-fold more yeast cells, than the estimated library size, were used for labeling and sorting. For the first round, library size was estimated by the transformation efficiency of the initial ligase library. For subsequent rounds, library size was taken to be the number of yeast cells collected during the previous sort. Protein expression was induced by inoculating saturated yeast culture (OD_{600} = 10) into the YPG medium at a 1:50 dilution and incubating at 30°C for 20 h. Each 1 mL of yeast cells (OD_{600} = 1) was pelleted at 12,000×*g* for 90 s and washed twice with 200 μL PBS containing 0.1% (m/v) bovine serum albumin (BSA). For blue-light-activated labeling, yeast cells from each 1 mL OD_{600} = 1 culture were resuspended in 200 μL PBSB with 100 μM Btn-NH_2. The cell suspension was irradiated with blue LED at a power of 15 mW/cm^2 for a certain time. For the directed evolution of $SOPP2^{I34V/I55V}$, we used 1-min irradiation in the 1st round selection and 5-s or 1-min irradiation for different subgroups in the second and third round of selection. For the BRET-assisted PL, yeast cells from each 1 mL OD_{600} = 1 culture were resuspended in 500 μL PBS with 1% (m/v) BSA, 100 μM Btn-NH_2, and 10 μM furimazine. The increased addition of BSA in this reaction system was intended to sufficiently quench the inter-cell labeling. The cell suspension was incubated in dark for 1 h at room temperature.

After the labeling reaction, yeast cells were pelleted at 12,000×*g* for 90 s and washed twice with 200 μL PBS containing 0.1% (m/v) BSA (PBSB). Subsequently, cells from each 1 mL OD_{600} = 1 culture were resuspended in 50 μL PBSB containing the primary antibody (200× diluted mouse anti-FLAG

antibody or 500× diluted mouse anti-V5 antibody) and incubated at room temperature for 1 h. The cells were washed twice with 200 μL PBSB, resuspended in 50 μL PBSB containing the secondary antibody (200× diluted goat anti-mouse-Alexa Fluor 488 and 200× diluted streptavidin-Alexa Fluor 647) and incubated in dark at room temperature for 30 min. After the immunostaining, yeast cells were washed twice with 200 μL PBSB and resuspended in 250 μL PBSB supplemented with 70 mg/L ampicillin and 50 mg/L kanamycin for FACS analysis. Gates were drawn to collect yeast cells with the highest activity/expression ratio, i.e., positive for AF488 signal and had high AF647 signal. After sorting, yeast cells were diluted with 2–3 mL SD-Ura-Trp medium and incubated at 37°C for 24–48 h. Part of the saturated yeast cell culture was resuspended in SD-Ura-Trp medium with 15% glycerol for cryopreservation. The remaining cell culture was either transferred to YPG medium to induce protein expression for the next round of selection, or it was lysed for plasmid extraction and sequencing.

For the directed evolution of SOPP2$^{I34V/I55V}$, mutant libraries were sorted on a BD FACS Aria III cell sorter (BD Bioscience). For the optimization of linkers, the linker truncation libraries and sequence randomized libraries were sorted on a BD FACS Aria SORP cell sorter (BD Bioscience). All the mutant characterization experiments conducted on yeast surface were analyzed by the CytoFLEX Flow Cytometer platform (Beckman Coulter). All data from FACS experiments were analyzed using FlowJo software.

Flow cytometry analysis of LAP mutants on HEK293T cell surface

For analyzing LAP mutants on HEK293T cell surface. HEK293T cells were transfected with tdTomato-P2A-CD40L-LAP mutants. Transfected HEK293T cells were digested with 0.05% trypsin for 1 min, collected and counted. 6×10^5 of CD40L-LAP cells were incubated with 100 μM BA probe and 20 μM furimazine in 1 mL DMEM medium supplemented with 10% fetal bovine serum at 37°C for 45 min; the reaction was performed in a 1.5-mL tube. The cells were collected by centrifugation for 2 min at 700 g, then washed 3 times with PBS. Then cells were stained with streptavidin-Alexa Fluor 647 (1:500) at room temperature for 30 min. After washing twice, cells were analyzed by BD LSRFortessa Cell Analyzer.

$^1O_2$ measurements

The SOSG probe was used for $^1O_2$ detection. To prepare a 5 mM stock solution, 100 μg SOSG powder was dissolved with 25 μL methanol. Then the SOSG solution was diluted with PBS to a concentration of 3 μM.

For $^1O_2$ measurement of SOPP2, SOPP3, and SOPP2$^{I34V/I55V}$, a PBS-based 30 μM FMN solution was prepared, and its absorbance at 440 nm was measured by NanoDrop 2000c (Thermo). Protein solutions of SOPP2, SOPP3, and SOPP2$^{I34V/I55V}$ were diluted with PBS to the same absorbance at 440 nm with 30 μM FMN. Equal volumes of SOSG and photocatalyst solutions were mixed and irradiated with blue light at 15 mW/cm^2 for 0, 15, 30, 45, and 60 s. The $^1O_2$ production was analyzed by measuring the fluorescence of SOSG oxidation products (Ex 504 nm, Em 535 nm). The absorbance at 440 nm was also recorded to analyze the photobleaching of photocatalysts.

For $^1O_2$ measurement of LAP and NanoLuc, 100 μL PBS solution containing 10 μM LAP or NanoLuc protein, 1 mM furimazine, and 1.5 μM SOSG was incubated at 37°C for 30 min, followed by centrifugation for 2 min at 15,000 g. The supernatant was analyzed by measuring the fluorescence of SOSG oxidation products (Ex 504 nm, Em 535 nm).

Cell viability assay

HEK293T cells targeting LAP to different subcellular locations were cultured into 96-well plates. After reaching 90% confluence, cells expressing ER lumen LAP were labeled with 50 μM Fz and 1 mM 3-EA for 2 h, cells expressing CD40L-LAP were labeled with 20 μM Fz and 100 μM BA for 45 min, and cells expressing ERM-LAP were labeled with 50 μM Fz and 10 mM PA for 1 h. Then the cells were washed by 100 μL PBS for two times and cultured in DMEM supplemented with 10% fetal bovine serum and maintained at 37°C with 5% CO_2 for 12 h. Cell viability was then measured by CellTiter 96 Aqueous One Solution Cell Proliferation Assay Kit (Promega, G3580).

BRET ratio measurement using purified proteins

To record luminescence spectra of LAP and SOPP2$^{I34V/I55V}$, 1 μM purified proteins was mixed with 75 μM furimazine in a complete DMEM without phenol red in 96-well plates with white walls (three repeats for each protein). After 3 min of reaction, luminescence spectra were recorded using a BioTek Synergy H1 Multimode Reader (Agilent). The BRET ratio calculation was performed as previously described.[53]

Generation of cell lines stably expressing LAP fusions

HEK293T and MC38 cells were cultured in DMEM supplemented with 10% fetal bovine serum and maintained at 37°C with 5% CO_2. To produce lentivirus, HEK293T cells cultured in 100-mm cell culture dishes were transfected at ~60% confluence using Lipofectamine 3000 reagent with the gene of interest in lentiviral vector pLX304 (6 μg), together with two packaging plasmids, dR8.91 (6 μg) and pVSV-G (4.2 μg). 48 h after transfection, the culture medium containing lentivirus was collected and filtered through a 0.45-μm filter. Then the virus was concentrated using Lenti-X Concentrator and resuspended in 2 mL of cell culture medium. 1 mL of the concentrated virus was mixed with 1 mL of fresh cell culture medium, then added to HEK293T cells or MC38 cells at ~50% confluence cultured in 6-well plates. Next, 48 h after lentivirus transfection, the culture medium was exchanged to fresh complete medium. For cell selection, HEK293T cell lines were cultured in 5 μg/mL of blasticidin-containing culture medium for 7 days, and MC38 cell lines were FACS sorted.

Proteome labeling with LAP-MS in living mammalian cells

Mammalian cell lines were cultured in 100-mm cell culture dishes, then labeled at ~90% confluence. Cells were incubated with 1 mM 3-EA and 50 μM furimazine in 10 mL DMEM supplemented with 10% fetal bovine serum at 37°C

for 2 h. Then, the cells were washed with cold PBS for three times and lysed immediately with RIPA reagent containing 1 × protease inhibitor. For one 100-mm culture dish of cells, 300 μL lysis buffer was used. Then the proteins were precipitated using methanol/chloroform protein precipitation method, followed by dissolving in 300 μL 0.5% SDS aqueous solution and mixing with 150 μL click cocktail (100 μM N_3-biotin, 667 μM $CuSO_4$, 1.3 mM BTTAA, and 2.5 mM sodium ascorbate). After 1-h reaction at room temperature, the proteins could be directly analyzed by western blot. Otherwise, the proteins could also be enriched and analyzed by western blot and LC-MS/MS.

Gel electrophoresis and western blot analysis

Protein samples were mixed with 5× protein loading buffer, followed by boiling at 95°C for 5 min. The samples were loaded to a 4%–20% gradient SDS-PAGE gel and analyzed by electrophoresis. For western blot analysis, the protein gel was transferred to a PVDF membrane under 230 mA for 1 h. The membrane was blocked with blocking buffer (5% BSA in TBST) at room temperature for 60 min and then incubated with streptavidin-HRP (1:5,000 dilution) in TBST at room temperature for 1 h. For anti-V5 or anti-HA western blot, the membrane was incubated with mouse anti-V5/anti-HA primary antibody (1:5,000 dilution) at room temperature for 60 min, followed by incubating anti-mouse secondary antibody conjugated with HRP (1:5,000 dilution) for 1 h. Antibodies used in this study can be found in Table S2. The membrane was washed by TBST three times after each step of incubation. The blots were imaged by ChemiDoc MP Imaging System (Bio-Rad).

Fluorescence microscopy

Cells were seeded on glass coverslips in 24-well plates at a density of ~70,000 cells per well. To improve the adherence of cells, glass coverslips were pretreated with 20% Corning Matrigel matrix diluted in DMEM (1:100) for 2 h at 37°C and washed with PBS once before use. After 24 h, cells were incubated with 1 mM 3-EA and 50 μM furimazine in DMEM supplemented with 10% fetal bovine serum at 37°C for 2 h. Thereafter, cells were washed with PBS once and fixed with cold methanol at −20°C for 10 min. Excess methanol was removed from fixed cells through washing with PBS three times. Next, 150 μL mixture of click reaction reagents was added to each well, containing 50 μM N_3-PEG_3-biotin (10 mM stock in DMSO), 2 mM $CuSO_4$, 1 mM BTTAA, and 0.5 mg/mL sodium ascorbate and incubated at room temperature for 30 min. After the click reaction, cells were washed with PBS three times and then blocked with 3% BSA in PBST (PBS containing 0.1% Tween 20) for 30 min at room temperature.

For immunostaining, cells were incubated with primary antibodies (mouse anti-V5 antibody at 1:5,000 dilution, mouse anti-HA antibody at 1:5,000 dilution, rabbit anti-Calnexin at 1:300 dilution) for 1 h at room temperature. After washing with PBST for three times, cells were incubated with secondary antibodies (goat anti-mouse Alexa Fluor 488 at 1:1,000 dilution, goat anti-rabbit Alexa Fluor 568 at 1:1,000 dilution), streptavidin-Alexa Fluor 637 (1:1,000 dilution), and DAPI (1:1,000 dilution) for 1 h at room temperature. After washing with PBST for three times, immunofluorescence images were collected with an inverted fluorescence microscope (Nikon-TiE) equipped with a spinning disk confocal unit (Yokogawa CSU-X1) and a scientific complementary metal-oxide semiconductor camera (Hamamatsu ORCA-Flash 4.0 v.2). The imaging equipment was controlled with a customized software written in LabVIEW v.15.0 (National Instruments).

Antibodies used in this study can be found in Table S2.

Protein enrichment and mass spectrometry sample preparation

For LC-MS/MS analysis, 4 mg of proteins purified after click reaction was used for enrichment. First, 30 μL of streptavidin agarose beads was centrifuged at 3,000×*g* for 2 min to remove the supernatant, followed by washing with 1 mL PBS for 3 times. Then the proteins dissolved in 500 μL 0.5% SDS in PBS were incubated with the beads for 3 h at room temperature with gentle rotation. After centrifugation, the supernatant was removed, and the beads were washed with 1 mL 0.5% SDS in PBS with 10-min gentle rotation, followed by washing with PBS for 6 times.

The beads were then resuspended by 500 μL 6 M urea in PBS, followed by addition of 12.5 μL 400 mM dithiothreitol (DTT) solution. After reactions at 37°C for 1 h, 12.5 μL 800 mM iodoacetamide (IAA) solution was added, followed by incubation at room temperature for 30 min in the dark. Agarose beads were washed four times with 1 mL 100 mM triethylammonium bicarbonate (TEAB) buffer and resuspended in 200 μL 100 mM TEAB. 0.5 μg sequencing-grade trypsin was then added for protein digestion by shaking at 1,200 rpm for 16 h at 37°C, and the released peptides in supernatant were collected after centrifugation and dried.

Dimethyl labeling was taken for quantitative proteomics. Peptide samples dissolved in 200 μL 100 mM TEAB were mixed with 8 μL 4% (v/v) CH_2O or 8 μL 4% (v/v) CD_2O, followed by addition of 8 μL 40 mg/mL $NaBH_3CN$ solution. After incubation at room temperature for 30 min, 32 μL 1% (v/v) ammonia solution was added to samples to stop the reactions. After 5-min incubation, 16 μL formic acid was then added. The light and heavy isotopically labeled samples were mixed and then dried. Finally, the peptide samples were fractionized by Pierce High pH Reverse Phase Peptide Fractionation Kit for LC-MS/MS analysis.

Liquid chromatography-tandem mass spectrometry

Peptides were separated using a loading column (100 μm × 2 cm) and a C18 separating capillary column (75 μm × 15 cm) packed in-house with Luna 3 μm C18(2) bulk packing material (Phenomenex, USA). The mobile phases (A: water with 0.1% formic acid and B: 80% acetonitrile with 0.1% formic acid) were driven and controlled by a Dionex Ultimate 3000 RPLC nano system (Thermo Fisher Scientific). The LC gradient was held at 2% for the first 8 min of the analysis, followed by an increase from 2% to 10% B from 8 to 9 min, an increase from 10% to 44% B from 9 to 123 min, and an increase from 44% to 99% B from 123 to 128 min.

For the samples analyzed by Orbitrap Fusion LUMOS Tribrid Mass Spectrometer, the precursors were ionized using an EASY-Spray ionization source (Thermo Fisher Scientific) held

Please cite this article in press as: Wang et al., Bioluminescence-activated proximity labeling for spatial multi-omics, Chem (2025), https://doi.org/10.1016/j.chempr.2025.102595

at +2.0 kV, compared with ground, and the inlet capillary temperature was held at 320°C. Survey scans of peptide precursors were collected in the Orbitrap from 350 to 1,600 Th with an AGC target of 400,000, a maximum injection time of 50 ms, RF lens at 30%, and a resolution of 60,000 at 200 *m/z*. Monoisotopic precursor selection was enabled for peptide isotopic distributions, precursors of z = 2–7 were selected for data-dependent MS/MS scans (with a resolution of 15,000) for 3 s of cycle time, and dynamic exclusion was set to 15 s with a ±10 ppm window set around the precursor monoisotope.

In HCD scans, an automated scan range determination was enabled. An isolation window of 1.6 Th was used to select precursor ions with the quadrupole. Product ions were collected in the Orbitrap with the first mass of 110 Th, an AGC target of 50,000, a maximum injection time of 30 ms, HCD collision energy at 30%, and a resolution of 15,000.

Mass spectrometry data analysis

All raw data were processed within the MaxQuant software package (version 1.6.1.0). Data were searched against the *Homo sapiens* or *Mus musculus* database downloaded from UniProt (www.uniprot.org). Half-tryptic termini and up to 1 missing trypsin cleavages were allowed. Carbamidomethylation at cysteine and isotopic modifications at lysine/N terminus were set as fixed modifications. Oxidation at methionine and acetylation of N terminus were set as variable modifications. Each of the biological replicates was analyzed separately. Contaminants and proteins identified as reverse hits were removed. Proteins with unique peptides < 2 or H/L ratio "NaN" were also removed. The quantification of light/heavy ratios was calculated with precursor mass tolerance of 20 ppm. The tolerance of the molecular weight of reporter ion on MS/MS is 0.003 Da.

Receiver operating characteristic analysis

For ER lumen proteome identified in MC38 cells and murine tumors, we performed ROC analysis to determine the cutoff ratios. According to the true-positive list defined in TurboID[13] work that contains 90 human ER proteins, we established a list containing 87 proteins that were included in the TurboID list but from mouse. The false positive list contains 7,296 proteins that are predicted to be non-secretory by Phobius[54] and also not annotated with the Gene Ontology terms including the following:

GO:0005783, GO:0005789, GO:0007029, GO:0030867, GO:0048237, GO:0061163, GO:0016320, GO:0030868, GO:0006983, GO:0000139, GO:0051645, GO:0031985, GO:0005796, GO:0005795, GO:0005794, GO:0007030, GO:0090168, GO:0005886, GO:0007009, GO:1903561, GO:0070062, GO:0005576, GO:0031012, GO:0005615, GO:0005769, GO:0035646, GO:0005765, GO:0090341, GO:0090340, GO:0005635, GO:0007084, GO:0007077, GO:0006998, GO:0051081, GO:0005641, GO:0031965, GO:0005637, GO:0071765, GO:0048471, GO:1905719, GO:0031982, GO:0006906, GO:0048278, GO:0032587, GO:0016021, GO:0005887, GO:0005768, GO:0071816, GO:0031526, GO:0005913, GO:0072546, GO:1990440, GO:0030968, GO:1902236, GO:1990441, GO:0034976, GO:0005788, GO:0005790, GO:1902237, GO:0070059, GO:0005786, GO:0005793, GO:0044322, GO:0098554, GO:0005791, GO:1902010, GO:0043001, GO:0005802, GO:0006888, GO:0006890, GO:0005801, GO:0012510, GO:0006892, GO:0042147, GO:0034499, GO:0032588, GO:0006895, GO:0030140, GO:0051684, GO:0000042, GO:0032580, GO:0030173, GO:0006891, GO:0030198, GO:0031668, GO:0010715, GO:0035426, GO:1903053, GO:1903551, GO:0005578, GO:1903055, GO:0001560, GO:0022617, GO:0006887, GO:0012505.

Protein and RNA labeling with LAP-MS in murine tumors

To generate solid tumors, 10^6 of MC38 cells stably expressing LAP in the ER lumen were subcutaneously implanted into 4- to 5-week-old C57BL/6N mice. When the tumor diameter reached ~7 mm (after 10–14 days), LAP labeling was initiated *in situ* by intratumoral injection of the 150 μL PBS solution containing 10 mM 3-EA probe and 4 mM furimazine. After a 2-h reaction, tumor tissues were isolated and lysed using RIPA buffer. The protein extraction, click, enrichment, western blot analysis, and LC-MS/MS analysis are as previously described. C57BL/6N mice were purchased from Charles River.

For *in vivo* RNA labeling, 10^6 of MC38 cells stably expressing ERM-LAP were subcutaneously implanted into 4- to 5-week-old C57BL/6N mice. When the tumor diameter reached ~7 mm (after 10–14 days), LAP labeling was initiated *in situ* by intratumoral injection of the 150 μL PBS solution containing 30 mM PA probe and 4 mM furimazine. After a 1-h reaction, tumor tissues were isolated and lysed using TRIzol reagent.

Cell-cell interaction labeling with LAP-CELL *in vitro*

For labeling of CD40-CD40L-mediated cell-cell interactions

HEK293T cells were transfected with tdTomato-P2A-CD40L-LAP, CD40-EGFP, and EGFP plasmid, respectively. Transfected HEK293T cells were digested with 0.05% trypsin for 1 min, collected, and counted. 4×10^5 of CD40L-LAP cells were mixed with 2×10^5 of CD40-EGFP cells or EGFP control cells, and then incubated with 100 μM BA probe and 20 μM furimazine in 1 mL DMEM supplemented with 10% fetal bovine serum at 37°C for 45 min; the reaction was performed in a 1.5-mL tube. The cells were collected by centrifugation for 2 min at 700 g, then washed 3 times with PBS. Then, cells were stained with streptavidin-Alexa Fluor 647 (1:500) at room temperature for 30 min. After washing twice, cell mixtures were analyzed by BD LSRFortessa Cell Analyzer.

For labeling of CD19 CAR-mediated cell-cell interactions

The HEK293T cell line stably expressing anti-CD19 CAR and cell membrane-localized LAP (IgK leader sequence-LAP-PDGFR transmembrane domain) was constructed as bait cells. We mixed different amounts of Raji and K562 cells: 10^3 of Raji cells and 10^5 of K562 cells, 10^4 of Raji cells and 10^5 of K562 cells, and 5×10^4 of Raji cells and 5×10^4 of K562 cells. Calcein AM staining was used for recognition of Raji or K562 cells. The above cell mixture was mixed with 4×10^5 of baited cells, followed by incubation with 100 μM BA probe and 20 μM furimazine in 1 mL DMEM supplemented with 10% fetal bovine serum at 37°C for 45 min, the reaction was performed in a 1.5-mL tube. The cells

were collected by centrifugation for 2 min at 700 g, then washed 3 times with PBS. Then, cells were stained with streptavidin-Alexa Fluor 647 (1:500) at room temperature for 30 min. After washing twice, cell mixtures were analyzed by BD LSRFortessa Cell Analyzer.

Cell-cell interaction labeling with LAP-CELL in living mice

HEK293T cells were transfected with tdTomato-P2A-CD40L-LAP, CD40-EGFP, and EGFP plasmid, respectively. Transfected HEK293T cells were digested with 0.05% trypsin for 1 min, collected, and counted. 4×10^5 of CD40L-LAP cells were mixed with 2×10^5 of CD40-EGFP cells or EGFP control cells, followed by intraperitoneal injection of them into 4- to 5-week-old C57BL/6N mice (volume: 500 μL). After 15-min incubation, 500 μL of PBS solution containing 300 μM furimazine and 1 mM BA probe was administrated into mice to trigger cellular labeling for 45 min, followed by cell isolation. The cells were collected by centrifugation for 2 min at 700 g, then washed 3 times with PBS. Then, cells were stained with streptavidin-Alexa Fluor 647 (1:500) at room temperature for 30 min. After washing twice, cell mixtures were analyzed by BD LSRFortessa Cell Analyzer. C57BL/6N mice were purchased from Charles River.

Transcriptome labeling and enrichment with LAP-seq in living mammalian cells

Cells stably expressing ERM-located LAP were seeded to 100-mm cell culture dishes, then labeled at ~90% confluence. Cells were incubated with 10 mM PA and 50 μM furimazine in DMEM supplemented with 10% fetal bovine serum at 37°C for 15–60 min. Then, the cells were washed with cold PBS thrice and lysed immediately with TRIzol reagent. Briefly, the homogenized sample was mixed and incubated with chloroform, and the upper aqueous phase was pipetted out and subjected to RNA precipitation by adding 100% isopropanol. The RNA pellet was washed with 75% ethanol and dissolved in RNase-free water. The purified RNA sample were treated with 1–2 μL DNaseI at 37°C for 30 min and then incubated with click reagents consisting of 0.1 mM biotin-azide, 2 mM THPTA, 0.5 mM $CuSO_4$, and 5 mM sodium ascorbate. After 10 min of CuAAC reaction at room temperature, RNAs were purified with RNA Clean & Concentrator kit and eluted with pre-warmed nuclease-free water. 50 μg of purified RNA was utilized for affinity enrichment.

20 μL of Dynabeads MyOne streptavidin C1 were washed three times with 200 μL B&W buffer (5 mM Tris pH 7.5, 1 M NaCl, 0.5 mM EDTA, 0.1% (v/v) Tween-20), twice with solution A (0.1 M NaOH, 0.05 M NaCl in nuclease-free water), once with solution B (0.1 M NaCl in nuclease-free water), and resuspended in 200 μL blocking buffer (1 mg/mL BSA, 1 mg/mL Yeast-tRNA in B&W buffer) on a shaker (1,200 rpm) for 2 h at 25°C. Thereafter, pre-blocked beads were washed three times with 200 μL B&W buffer. Extracted RNAs (around 50 μg) were mixed with an equal volume of 2× B&W buffer (10 mM Tris pH 7.5, 2 M NaCl, 1 mM EDTA, 0.2% (v/v) Tween-20) before incubating with the pre-blocked beads on a shaker (1,200 rpm) for 45 min at 25°C to allow binding of biotinylated RNAs. The supernatant was discarded, and the beads were washed three times with 200 μL B&W buffer, twice with 200 μL Urea buffer (4 M Urea, 0.1% (w/v) SDS in PBS), and twice with 200 μL PBS. The beads were finally resuspended in 50 μL Elution buffer (95% formamide, 10 mM EDTA, 1.5 mM D-biotin), heated at 50°C for 5 min and then at 90°C for 5 min. The supernatant containing eluted biotinylated RNAs was transferred to a 1.5-mL Eppendorf tube and mixed with 1 mL TRIzol reagent to extract RNA. Each sample was added with 200 μL chloroform and mixed vigorously, followed by centrifugation for 15 min at 4°C, 12,000 *g*. The aqueous phase with dissolved RNAs was transferred to a new tube, added with 500 μL isopropanol and 20 μg glycogen, and then incubated at -20°C overnight to precipitate RNA. The sediment was washed with 1 mL 75% (v/v) ethanol and dissolved into 10 μL of nuclease-free water.

Dot blot analysis of enriched RNA

Equal volume of purified biotinylated RNA was loaded onto Immobilon-Ny + membrane and crosslinked to the membrane by an ultraviolet crosslinker. The membrane was blocked with 5% BSA in PBST (PBS containing 0.1% Tween-20) at room temperature for 1 h and incubated with streptavidin-HRP in PBST at room temperature for 1 h. The membrane was washed three times with PBST for 10 min each time, incubated in Clarity Western ECL Substrate and then imaged on a ChemiDoc imaging system (Bio-Rad).

RT-qPCR analysis of enriched RNA

For each sample, 1 μg of input RNA and 3 μL of enriched RNA were reverse transcribed with random primers and ProtoScript II in 20 μL reaction buffer, according to the manufacturer's instructions. The input and enriched cDNAs were aliquoted into four tubes (for four genes) as templates for qPCR. The templates were mixed with PowerUp SYBR Green Master Mix and primers and then quantified by ABI StepOne Plus system. C_t values were averaged from four replicate measurements. Negative controls without furimazine were treated in the same manner as the sample and were used here to calculate enrichment FC: $2^{\Delta Ct\_control - \Delta Ct\_label}$, where $\Delta C_t = C_t^{Enrich} - C_t^{Input}$.

Library construction for next-generation sequencing

NEBNext Ultra II RNA Library Prep Kit for Illumina (NEB, E7770) was used for cDNA library construction. 100 ng input and 5 μL enriched (label or omitting furimazine) RNAs were fragmentated to ~300 nt in the presence of 1 μL Random primer and 4 μL First Strand Synthesis Reaction Buffer at 94°C. Then the fragmentated RNAs were mixed with 2 μL First Strand Synthesis Enzyme Mix and 8 μL nuclease-free water for reverse transcription (25°C for 10 min, 42°C for 25 min, and 70°C for 15 min). Then 8 μL of Second Strand Synthesis Reaction Buffer (10×), 4 μL of Second Strand Synthesis Enzyme Mix, and 48 μL water were added to the first strand reaction product for second strand cDNA synthesis and incubated for 1 h at 16°C. The double-stranded cDNA was purified with 1.8× VAHTS DNA Clean Beads and eluted by 50 μL 0.1× TE buffer. For end prep, the eluted cDNA was mixed with 7 μL of End Prep Reaction Buffer, 3 μL Enzyme Mix and incubated at 20°C for 30 min and at 65°C for 30 min. For adaptor ligation, 2.5 μL diluted adaptor, 1 μL ligation Enhancer, and 30 μL Ligation Master Mix were added to the end prepped DNA and incubated at 20°C for 20 min. The ligated cDNA was purified

using 0.9× VAHTS DNA Clean Beads, then amplified by PCR, and purified again with 0.9× VAHTS DNA Clean Beads. The input samples, label_Enrich samples, and control_Enrich samples were amplified for 11, 14, and 16 cycles, respectively. The quality of libraries was tested using Agilent D1000 ScreenTape System. To further refine the library size distribution, two rounds of size selection were performed using 0.6–0.7× and 0.3× VAHTS DNA Clean Beads, according to the manufacturer's instructions. Finally, the cDNA libraries were sequenced on the Illumina HiSeq X Ten platform, generating 150 bp paired-end reads.

Next-generation sequencing data analysis

Cutadapt[55] (v.1.18) was utilized first for adaptor sequence removal. Then the reads were mapped by hisat2[56] (v.2.1.0) against the human genome assembly GRCh38 (hg38) downloaded from Ensembl. Using the gene annotation (v.87) downloaded from Ensembl, the mapped reads were counted by HTSeq[57] (v.0.7.2) with the option "–stranded no." Then, differential expression analysis was carried out by DESeq2[38] (v.1.16.1).

HEK293T ERM dataset was defined with the cutoff of $\log_2$FC (label vs. control) $>$ 1 and $p_{adj} < 0.05$. True-positive human secretary pathway mRNAs were referred to the CAP-seq work. The MC38 ERM RNA dataset was defined as the overlap between the enriched targets in two differential analyses by DESeq2: post- vs. pre-enrichment of RNA labeled with ERM-LAP, and post-enriched RNA labeled with ERM-LAP vs. RNA from negative control omitting furimazine. The cutoffs were set as $\log_2$FC $>$ 0.3 and $p_{adj} < 0.05$. True-positive mouse secretary pathway mRNAs were defined as the ensemble of genes whose Gene Ontology cellular component (GOCC) annotations contain the following words that related to "secretory pathway": "endoplasmic reticulum," "Golgi," "plasma membrane," "extracellular," "endosome," "lysosome," "nuclear envelope," "nuclear membrane," "perinuclear region of cytoplasm," and "vesicle."

RESOURCE AVAILABILITY

Lead contact

Further information and requests for resources and reagents should be directed to and will be fulfilled by the lead contact, Peng Zou (zoupeng@pku.edu.cn).

Materials availability

All materials generated in this study are available from the lead contact without restriction.

Data and code availability

The proteomic data generated in this study have been deposited in the ProteomeXchange database under accession code PXD055458. The RNA-sequencing data generated in this study have been deposited in the National Center for Biotechnology Information Gene Expression Omnibus under accession code GSE276085. All data supporting this study are available in the manuscript and supplemental information.

ACKNOWLEDGMENTS

This work was supported by the National Natural Science Foundation of China (32088101), the Ministry of Science and Technology (2022YFA1304700), and Beijing National Laboratory for Molecular Sciences (BNLMS-CXXM-202403). Y.L. is supported by the Knowledge Innovation Program of Wuhan-Shuguang Project (2023020201020353). P.Z. is sponsored by a Bayer Investigator Award. We thank X. Zhou and L. Kong for advice on mass spec sample preparation; S. Zhao, Z. Ren, and G. Wang for advice on cDNA library preparation; G. Yuan and Y. Fu for providing BA probe; S. Liu for providing plasmids for cell-cell interaction study; and all lab members for helpful discussions. The measurements of mass spectrometry were performed at the Analytical Instrumentation Center of Peking University. The help from PKUAIC (Dr. Wen Zhou) is acknowledged.

AUTHOR CONTRIBUTIONS

P.Z., P.R.C., and Y.L. conceived the project. P.Z., P.R.C., Y.L., R.W., and Y.F. designed the experiments. R.W., Y.F., Y.L., and Y.H. performed the experiments. P.Z., R.W., and Y.F. wrote the manuscript with input from all authors.

DECLARATION OF INTERESTS

The authors declare no competing interests.

SUPPLEMENTAL INFORMATION

Supplemental information can be found online at https://doi.org/10.1016/j.chempr.2025.102595.

Received: November 4, 2024
Revised: March 30, 2025
Accepted: April 27, 2025
Published: May 19, 2025

REFERENCES

1. Thul, P.J., Åkesson, L., Wiking, M., Mahdessian, D., Geladaki, A., Ait Blal, H., Alm, T., Asplund, A., Björk, L., Breckels, L.M., et al. (2017). A subcellular map of the human proteome. Science *356*, eaal3321. https://doi.org/10.1126/science.aal3321.
2. Benham, A.M. (2012). Protein secretion and the endoplasmic reticulum. Cold Spring Harb. Perspect. Biol. *4*, a012872. https://doi.org/10.1101/cshperspect.a012872.
3. Hofmann, S., Kedersha, N., Anderson, P., and Ivanov, P. (2021). Molecular mechanisms of stress granule assembly and disassembly. Biochim. Biophys. Acta Mol. Cell Res. *1868*, 118876. https://doi.org/10.1016/j.bbamcr.2020.118876.
4. Hilligan, K.L., and Ronchese, F. (2020). Antigen presentation by dendritic cells and their instruction of CD4+ T helper cell responses. Cell. Mol. Immunol. *17*, 587–599. https://doi.org/10.1038/s41423-020-0465-0.
5. Kim, Y.S., Choi, J., and Yoon, B.E. (2020). Neuron-glia interactions in neurodevelopmental disorders. Cells *9*, 2176. https://doi.org/10.3390/cells9102176.
6. Hinshaw, D.C., and Shevde, L.A. (2019). The tumor microenvironment innately modulates cancer progression. Cancer Res. *79*, 4557–4566. https://doi.org/10.1158/0008-5472.CAN-18-3962.
7. O'Donnell, J.S., Teng, M.W.L., and Smyth, M.J. (2019). Cancer immunoediting and resistance to T cell-based immunotherapy. Nat. Rev. Clin. Oncol. *16*, 151–167. https://doi.org/10.1038/s41571-018-0142-8.
8. Hetz, C., and Saxena, S. (2017). ER stress and the unfolded protein response in neurodegeneration. Nat. Rev. Neurol. *13*, 477–491. https://doi.org/10.1038/nrneurol.2017.99.
9. Rhee, H.W., Zou, P., Udeshi, N.D., Martell, J.D., Mootha, V.K., Carr, S.A., and Ting, A.Y. (2013). Proteomic mapping of mitochondria in living cells via spatially restricted enzymatic tagging. Science *339*, 1328–1331. https://doi.org/10.1126/science.1230593.
10. Lam, S.S., Martell, J.D., Kamer, K.J., Deerinck, T.J., Ellisman, M.H., Mootha, V.K., and Ting, A.Y. (2015). Directed evolution of APEX2 for electron microscopy and proximity labeling. Nat. Methods *12*, 51–54. https://doi.org/10.1038/nmeth.3179.

11. Qin, W., Cho, K.F., Cavanagh, P.E., and Ting, A.Y. (2021). Deciphering molecular interactions by proximity labeling. Nat. Methods *18*, 133–143. https://doi.org/10.1038/s41592-020-01010-5.

12. Roux, K.J., Kim, D.I., Raida, M., and Burke, B. (2012). A promiscuous biotin ligase fusion protein identifies proximal and interacting proteins in mammalian cells. J. Cell Biol. *196*, 801–810. https://doi.org/10.1083/jcb.201112098.

13. Branon, T.C., Bosch, J.A., Sanchez, A.D., Udeshi, N.D., Svinkina, T., Carr, S.A., Feldman, J.L., Perrimon, N., and Ting, A.Y. (2018). Efficient proximity labeling in living cells and organisms with TurboID. Nat. Biotechnol. *36*, 880–887. https://doi.org/10.1038/nbt.4201.

14. Liu, Y., Zeng, R., Wang, R., Weng, Y., Wang, R., Zou, P., and Chen, P.R. (2021). Spatiotemporally resolved subcellular phosphoproteomics. Proc. Natl. Acad. Sci. USA *118*, e2025299118. https://doi.org/10.1073/pnas.2025299118.

15. Lee, S.Y., Cheah, J.S., Zhao, B., Xu, C., Roh, H., Kim, C.K., Cho, K.F., Udeshi, N.D., Carr, S.A., and Ting, A.Y. (2023). Engineered allostery in light-regulated LOV-Turbo enables precise spatiotemporal control of proximity labeling in living cells. Nat. Methods *20*, 908–917. https://doi.org/10.1038/s41592-023-01880-5.

16. Al Mismar, R., Samavarchi-Tehrani, P., Seale, B., Kasmaeifar, V., Martin, C.E., and Gingras, A.C. (2024). Extracellular proximal interaction profiling by cell surface-targeted TurboID reveals LDLR as a partner of liganded EGFR. Sci. Signal. *17*, eadl6164. https://doi.org/10.1126/scisignal.adl6164.

17. Pasqual, G., Chudnovskiy, A., Tas, J.M.J., Agudelo, M., Schweitzer, L.D., Cui, A., Hacohen, N., and Victora, G.D. (2018). Monitoring T cell-dendritic cell interactions in vivo by intercellular enzymatic labelling. Nature *553*, 496–500. https://doi.org/10.1038/nature25442.

18. Ge, Y., Chen, L., Liu, S., Zhao, J., Zhang, H., and Chen, P.R. (2019). Enzyme-mediated intercellular proximity labeling for detecting cell-cell interactions. J. Am. Chem. Soc. *141*, 1833–1837. https://doi.org/10.1021/jacs.8b10286.

19. Fang, Y., and Zou, P. (2023). Photocatalytic proximity labeling for profiling the subcellular organization of biomolecules. ChemBioChem *24*, e202200745. https://doi.org/10.1002/cbic.202200745.

20. Shu, X., Lev-Ram, V., Deerinck, T.J., Qi, Y., Ramko, E.B., Davidson, M.W., Jin, Y., Ellisman, M.H., and Tsien, R.Y. (2011). A genetically encoded tag for correlated light and electron microscopy of intact cells, tissues, and organisms. PLOS Biol. *9*, e1001041. https://doi.org/10.1371/journal.pbio.1001041.

21. Hall, M.P., Unch, J., Binkowski, B.F., Valley, M.P., Butler, B.L., Wood, M.G., Otto, P., Zimmerman, K., Vidugiris, G., Machleidt, T., et al. (2012). Engineered luciferase reporter from a deep sea shrimp utilizing a novel imidazopyrazinone substrate. ACS Chem. Biol. *7*, 1848–1857. https://doi.org/10.1021/cb3002478.

22. Bacart, J., Corbel, C., Jockers, R., Bach, S., and Couturier, C. (2008). The BRET technology and its application to screening assays. Biotechnol. J. *3*, 311–324. https://doi.org/10.1002/biot.200700222.

23. Wang, P., Tang, W., Li, Z., Zou, Z., Zhou, Y., Li, R., Xiong, T., Wang, J., and Zou, P. (2019). Mapping spatial transcriptome with light-activated proximity-dependent RNA labeling. Nat. Chem. Biol. *15*, 1110–1119. https://doi.org/10.1038/s41589-019-0368-5.

24. Ding, T., Zhu, L., Fang, Y., Liu, Y., Tang, W., and Zou, P. (2020). Chromophore-assisted proximity labeling of DNA reveals chromosomal organization in living cells. Angew. Chem. Int. Ed. Engl. *59*, 22933–22937. https://doi.org/10.1002/anie.202005486.

25. Zheng, F., Yu, C., Zhou, X., and Zou, P. (2023). Genetically encoded photocatalytic protein labeling enables spatially-resolved profiling of intracellular proteome. Nat. Commun. *14*, 2978. https://doi.org/10.1038/s41467-023-38565-8.

26. Zhai, Y., Huang, X., Zhang, K., Huang, Y., Jiang, Y., Cui, J., Zhang, Z., Chiu, C.K.C., Zhong, W., and Li, G. (2022). Spatiotemporal-resolved protein networks profiling with photoactivation dependent proximity labeling. Nat. Commun. *13*, 4906. https://doi.org/10.1038/s41467-022-32689-z.

27. Hananya, N., Ye, X., Koren, S., and Muir, T.W. (2023). A genetically encoded photoproximity labeling approach for mapping protein territories. Proc. Natl. Acad. Sci. USA *120*, e2219339120. https://doi.org/10.1073/pnas.2219339120.

28. Shramova, E.I., Chumakov, S.P., Shipunova, V.O., Ryabova, A.V., Telegin, G.B., Kabashin, A.V., Deyev, S.M., and Proshkina, G.M. (2022). Genetically encoded BRET-activated photodynamic therapy for the treatment of deep-seated tumors. Light Sci. Appl. *11*, 38. https://doi.org/10.1038/s41377-022-00729-4.

29. Westberg, M., Holmegaard, L., Pimenta, F.M., Etzerodt, M., and Ogilby, P.R. (2015). Rational design of an efficient, genetically encodable, protein-encased singlet oxygen photosensitizer. J. Am. Chem. Soc. *137*, 1632–1642. https://doi.org/10.1021/ja511940j.

30. Westberg, M., Bregnhøj, M., Etzerodt, M., and Ogilby, P.R. (2017). No photon wasted: an efficient and selective singlet oxygen photosensitizing protein. J. Phys. Chem. B *121*, 9366–9371. https://doi.org/10.1021/acs.jpcb.7b07831.

31. Abramson, J., Adler, J., Dunger, J., Evans, R., Green, T., Pritzel, A., Ronneberger, O., Willmore, L., Ballard, A.J., Bambrick, J., et al. (2024). Accurate structure prediction of biomolecular interactions with AlphaFold 3. Nature *630*, 493–500. https://doi.org/10.1038/s41586-024-07487-w.

32. Efremova, M., Rieder, D., Klepsch, V., Charoentong, P., Finotello, F., Hackl, H., Hermann-Kleiter, N., Löwer, M., Baier, G., Krogsdam, A., Trajanoski, Z., et al. (2018). Targeting immune checkpoints potentiates immunoediting and changes the dynamics of tumor evolution. Nat. Commun. *9*, 32. https://doi.org/10.1038/s41467-017-02424-0.

33. Juneja, V.R., McGuire, K.A., Manguso, R.T., LaFleur, M.W., Collins, N., Haining, W.N., Freeman, G.J., and Sharpe, A.H. (2017). PD-L1 on tumor cells is sufficient for immune evasion in immunogenic tumors and inhibits CD8 T cell cytotoxicity. J. Exp. Med. *214*, 895–904. https://doi.org/10.1084/jem.20160801.

34. Laman, J.D., Claassen, E., and Noelle, R.J. (2017). Functions of CD40 and its ligand, gp39 (CD40L). Crit. Rev. Immunol. *37*, 371–420. https://doi.org/10.1615/CritRevImmunol.v37.i2-6.100.

35. Chen, R., Chen, L., Wang, C., Zhu, H., Gu, L., Li, Y., Xiong, X., Chen, G., and Jian, Z. (2023). CAR-T treatment for cancer: prospects and challenges. Front. Oncol. *13*, 1288383. https://doi.org/10.3389/fonc.2023.1288383.

36. Jogalekar, M.P., Rajendran, R.L., Khan, F., Dmello, C., Gangadaran, P., and Ahn, B.C. (2022). CAR T-Cell-Based gene therapy for cancers: new perspectives, challenges, and clinical developments. Front. Immunol. *13*, 925985. https://doi.org/10.3389/fimmu.2022.925985.

37. Denlinger, N., Bond, D., and Jaglowski, S. (2022). CAR T-cell therapy for B-cell lymphoma. Curr. Probl. Cancer *46*, 100826. https://doi.org/10.1016/j.currproblcancer.2021.100826.

38. Love, M.I., Huber, W., and Anders, S. (2014). Moderated estimation of fold change and dispersion for RNA-seq data with DESeq2. Genome Biol. *15*, 550. https://doi.org/10.1186/s13059-014-0550-8.

39. Jan, C.H., Williams, C.C., and Weissman, J.S. (2014). Principles of ER cotranslational translocation revealed by proximity-specific ribosome profiling. Science *346*, 1257521. https://doi.org/10.1126/science.1257521.

40. Kaewsapsak, P., Shechner, D.M., Mallard, W., Rinn, J.L., and Ting, A.Y. (2017). Live-cell mapping of organelle-associated RNAs via proximity biotinylation combined with protein-RNA crosslinking. eLife *6*, e29224. https://doi.org/10.7554/eLife.29224.

41. Zhang, Y., Liu, Z., Zhou, N., Guo, F., Guo, H., Chen, X., Qin, S., Chen, P.R., and Fan, X. (2025). In situ lysosomal proteomics enabled by bioorthogonal photocatalytic proximity labelling. Nat. Catal. *8*, 162–177. https://doi.org/10.1038/s41929-025-01298-6.

42. Geri, J.B., Oakley, J.V., Reyes-Robles, T., Wang, T., McCarver, S.J., White, C.H., Rodriguez-Rivera, F.P., Parker, D.L., Jr., Hett, E.C., Fadeyi, O.O., et al. (2020). Microenvironment mapping via Dexter energy transfer on immune cells. Science *367*, 1091–1097. https://doi.org/10.1126/science.aay4106.

43. Buksh, B.F., Knutson, S.D., Oakley, J.V., Bissonnette, N.B., Oblinsky, D. G., Schwoerer, M.P., Seath, C.P., Geri, J.B., Rodriguez-Rivera, F.P., Parker, D.L., et al. (2022). μMap-Red: proximity labeling by red light photocatalysis. J. Am. Chem. Soc. *144*, 6154–6162. https://doi.org/10.1021/jacs.2c01384.

44. Huang, Z., Liu, Z., Xie, X., Zeng, R., Chen, Z., Kong, L., Fan, X., and Chen, P.R. (2021). Bioorthogonal photocatalytic decaging-enabled mitochondrial proteomics. J. Am. Chem. Soc. *143*, 18714–18720. https://doi.org/10.1021/jacs.1c09171.

45. Li, Y., Aggarwal, M.B., Nguyen, K., Ke, K., and Spitale, R.C. (2017). Assaying RNA localization *in situ* with spatially restricted nucleobase oxidation. ACS Chem. Biol. *12*, 2709–2714. https://doi.org/10.1021/acschembio.7b00519.

46. Engel, K.L., Lo, H.G., Goering, R., Li, Y., Spitale, R.C., and Taliaferro, J.M. (2022). Analysis of subcellular transcriptomes by RNA proximity labeling with Halo-seq. Nucleic Acids Res. *50*, e24. https://doi.org/10.1093/nar/gkab1185.

47. Tamura, T., Takato, M., Shiono, K., and Hamachi, I. (2020). Development of a photoactivatable proximity labeling method for the identification of nuclear proteins. Chem. Lett. *49*, 145–148. https://doi.org/10.1246/cl.190804.

48. Liu, H., Luo, H., Xue, Q., Qin, S., Qiu, S., Liu, S., Lin, J., Li, J.P., and Chen, P.R. (2022). Antigen-specific T cell detection via photocatalytic proximity cell labeling (PhoXCELL). J. Am. Chem. Soc. *144*, 5517–5526. https://doi.org/10.1021/jacs.2c00159.

49. Oslund, R.C., Reyes-Robles, T., White, C.H., Tomlinson, J.H., Crotty, K.A., Bowman, E.P., Chang, D., Peterson, V.M., Li, L., Frutos, S., et al. (2022). Detection of cell-cell interactions via photocatalytic cell tagging. Nat. Chem. Biol. *18*, 850–858. https://doi.org/10.1038/s41589-022-01044-0.

50. Zhang, Y., Liu, S., Guo, F., Qin, S., Zhou, N., Liu, Z., Fan, X., and Chen, P.R. (2024). Bioorthogonal quinone methide decaging enables live-cell quantification of tumor-specific immune interactions. J. Am. Chem. Soc. *146*, 15186–15197. https://doi.org/10.1021/jacs.4c02052.

51. Inutsuka, A., Kimizuka, N., Takanohashi, N., Yakabu, H., and Onaka, T. (2020). Visualization of a blue light transmission area in living animals using light-induced nuclear translocation of fluorescent proteins. Biochem. Biophys. Res. Commun. *522*, 138–143. https://doi.org/10.1016/j.bbrc.2019.11.023.

52. Li, T., Chen, X., Qian, Y., Shao, J., Li, X., Liu, S., Zhu, L., Zhao, Y., Ye, H., and Yang, Y. (2021). A synthetic BRET-based optogenetic device for pulsatile transgene expression enabling glucose homeostasis in mice. Nat. Commun. *12*, 615. https://doi.org/10.1038/s41467-021-20913-1.

53. Proshkina, G.M., Shramova, E.I., Shilova, O.N., Ryabova, A.V., and Deyev, S.M. (2018). Phototoxicity of flavoprotein miniSOG induced by bioluminescence resonance energy transfer in genetically encoded system NanoLuc-miniSOG is comparable with its LED-excited phototoxicity. J. Photochem. Photobiol. B *188*, 107–115. https://doi.org/10.1016/j.jphotobiol.2018.09.006.

54. Käll, L., Krogh, A., and Sonnhammer, E.L.L. (2004). A combined transmembrane topology and signal peptide prediction method. J. Mol. Biol. *338*, 1027–1036. https://doi.org/10.1016/j.jmb.2004.03.016.

55. Martin, M. (2011). Cutadapt removes adapter sequences from high-throughput sequencing reads. EMBnet. j. *17*, 10–12. https://doi.org/10.14806/ej.17.1.200.

56. Kim, D., Langmead, B., and Salzberg, S.L. (2015). HISAT: a fast spliced aligner with low memory requirements. Nat. Methods *12*, 357–360. https://doi.org/10.1038/nmeth.3317.

57. Anders, S., Pyl, P.T., and Huber, W. (2015). HTSeq–a Python framework to work with high-throughput sequencing data. Bioinformatics *31*, 166–169. https://doi.org/10.1093/bioinformatics/btu638.